Crystal Growth of BCC Titanium from the Melt and Interfacial Properties: A Molecular Dynamics Simulation Study

R. E. Rozas,[1, a)] L. G. MacDowell,[2] P. G. Toledo,[3] and J. Horbach[4]
[1)]*Department of Physics, University of Bío-Bío, Av. Collao 1202, PO Box 5-C, Concepción, Chile*
[2)]*Departamento de Química Física, Universidad Complutense de Madrid, Madrid 28040, Spain*
[3)]*Chemical Engineering Department and Surface Analysis Laboratory (ASIF), University of Concepción, PO Box 160-C, Correo 3, Concepción, Chile*
[4)]*Institut für Theoretische Physik II: Weiche Materie, Heinrich-Heine-Universität Düsseldorf, Universitätsstraße 1, D-40225 Düsseldorf, Germany*

The crystal growth kinetics as well as interfacial properties of Titanium (Ti) are studied, using molecular dynamics (MD) computer simulation. The interactions between the Ti atoms are modelled via an embedded atom method (EAM) potential. First, the free solidification method (FSM) is used to determine the melting temperature T_m at zero pressure where the transition from liquid to body-centered cubic (bcc) crystal occurs. From the simulations with the FSM, also the kinetic growth coefficients are determined for different orientations of the crystal, analyzing how the coupling to the thermostat affects the estimates of the growth coefficients. At T_m, anisotropic interfacial stiffnesses and free energies as well as kinetic growth coefficients are determined from capillary wave fluctuations. The so obtained growth coefficients from equilibrium fluctuations and without the coupling of the system to a thermostat agree well with those extracted from the FSM calculations.

PACS numbers: 61.25.Mv, 61.20.Ja, 02.70.Ns, 64.70.mf

I. INTRODUCTION

In metallic systems, the continuum modelling of solidification processes from the melt requires input parameters that are hardly accessible from experiments[1,2]. Among these parameters are in particular interfacial free energies, γ, and stiffnesses, $\tilde{\gamma}$, of solid-liquid interfaces as well as kinetic growth coefficients, μ. These parameters are tensorial quantities that depend on the orientation of the crystal with respect to the liquid. As a matter of fact, the degree of their anisotropy determines the morphology of growing crystals[1,2] and thus, the knowledge of γ, $\tilde{\gamma}$, and μ is essential for a fundamental understanding and controlled design of crystallization processes from the melt. Due to the lack of experimental data, particle-based simulation techniques such as molecular dynamics (MD) computer simulations play an important role to determine interfacial properties and growth coefficients for metallic systems.

Many MD simulation studies on crystal-liquid interfaces and crystalline growth in metals have been devoted to systems where close-packed structures such as face-centered cubic (fcc) crystals are formed (see, e.g., Refs.[3–15]). However, similar systematic studies of systems with a body-centered cubic (bcc) structure are rare[16–24]. In this context, Titanium (Ti) is a very interesting material that can be seen as a paradigm for a one-component metal with a high-temperature bcc phase. Nevertheless, information of solid-liquid interfacial properties and kinetic growth coefficients of Ti from MD simulations are, to the best of our knowledge, not available. In this work, we are aiming at filling this gap and present a systematic investigation of an embedded atom method (EAM) model of Ti via MD simulation.

A central technique that we use in this work is the capillary fluctuation method[3,6–9,13,15,25]. In this method, inhomogeneous systems with crystal-liquid interfaces at coexistence are prepared, followed by an analysis of the long-wavelength height fluctuations of the interfaces. The capillary fluctuation method provides reliable estimates of interfacial stiffnesses and interfacial free energies. Also kinetic growth coefficients μ can be obtained from the capillary fluctuation method. To this end, one computes μ from a time- and wavenumber-dependent height-height correlation function in the hydrodynamic limit, i.e. at long wavelengths and long times. Here, we follow the methodology that has been proposed by Benet *et al.*[15].

We also determine kinetic growth coefficients from the free solidification method (FSM) that has been widely used to determine μ (see, e.g., Ref.[11] and references therein). Unlike the calculation of μ via the capillary fluctuation method, FSM is based on non-equilibrium MD simulations and requires the coupling of the system to a thermostat. This coupling can lead to artifacts and therefore, in this work, we systematically vary the coupling to the thermostat to elucidate how the thermostat affects the estimate of kinetic growth coefficients. We show that by an appropriate choice of the thermostat coupling parameter, one obtains reliable estimates of μ, in agreement with those computed from the equilibrium fluctuations, i.e. via the capillary fluctuation method.

The rest of the manuscript is organized as follows. In the next section (Sec. 2), we introduce the interaction model potential that we have used in this work. Section 3 analyzes the temperature dependence of the density and other properties of the bulk bcc and liquid phase at zero pressure. Then, Sec. 4 presents the results for kinetic growth coefficients via FSM,

[a)]Electronic mail: rrozas@ubiobio.cl

where we systematically vary the coupling to the required thermostat. Interfacial stiffnesses and free energies and their anisotropies are computed in Sec. 5 using the capillary fluctuation method. This method is employed in Sec. 6 to compute kinetic growth coefficients and compare them to those obtained by FSM. Finally, in Sec. 7 we summarize the results and draw some conclusions.

II. MODEL POTENTIAL FOR TITANIUM

We use an EAM potential model to describe the interactions between the atoms in Ti. Although this model takes into account many-body interactions, its computational load is similar to that of a pair potential.

Consider a system of N particles. Then, the EAM potential energy of an atom i can be written as

$$U_i = \sum_{j\neq i} \Phi(r_{ij}) + F(\rho_i^{\mathrm{h}}) \tag{1}$$

where Φ is a pair potential that depends on the distance $r_{ij} = |\mathbf{r}_i - \mathbf{r}_j|$ between particle i at position $\mathbf{r}_i$ and particle j at position $\mathbf{r}_j$. The function F is an embedding energy and depends on the host electronic density ρ_i^{h} of particle i which is defined by

$$\rho_i^{\mathrm{h}} = \sum_{j\neq i} \rho^{\mathrm{at}}(r_{ij})\,, \tag{2}$$

with the electron-density ρ^{at} being solely a function of r_{ij}.

Based on information from experiment and *ab initio* calculations, Zope and Mishin[26] have derived an EAM potential for Ti where the pair potential Φ, the electron-density ρ^{at} and the embedding energy F are cut off at a distance $r_c = 5.193995\,\text{Å}$ i.e. for $r > r_c$ these functions are set to zero. In the model of Zope and Mishin, the potential Φ for a pair of particles separated by a distance r is given by

$$\Phi(r) = \{V_0 \mathrm{e}^{-\beta_1 r_1} + V_0'[\mathrm{e}^{-2\beta_2(r-r_1')} - 2\mathrm{e}^{\beta_2(r-r_1')}] + \delta\}\,\psi\left(\frac{r-r_c}{h}\right) \tag{3}$$

where the function ψ ensures that the function $\Phi(r)$ vanishes smoothly at $r = r_c$. It is defined as

$$\psi(u) = \begin{cases} u^4/(1+u^4) & \text{for} \quad u < 0 \\ 0 & \text{for} \quad u \geq 0\,. \end{cases} \tag{4}$$

The parameters of the potential in Eq. (3) are given by $V_0 = -3.401822 \cdot 10^6\,\text{eV}$, $V_0' = 0.161862\,\text{eV}$, $r_1 = -8.825787\,\text{Å}$, $\beta_1 = 5.933482\,\text{Å}^{-1}$, $r_1' = 3.142920\,\text{Å}$, $\beta_2 = 2.183169\,\text{Å}^{-1}$, $\delta = -0.601156 \cdot 10^{-1}\,\text{eV}$, and $h = 0.675729\,\text{Å}$.

For the electron-density $\rho^{\mathrm{at}}(r)$, the same smoothing function ψ and cut off r_c as for Φ is used. This function is given by

$$\rho^{\mathrm{at}}(r) = \left[A\mathrm{e}^{-\alpha_1(r-r_0)^2} + \mathrm{e}^{-\alpha_2(r-r_0')}\right]\psi\left(\frac{r-r_c}{h}\right). \tag{5}$$

Here, the parameters are $A = 3.656883 \cdot 10^2$, $r_0 = -1.169053 \cdot 10^1\,\text{Å}$, $r_0' = -2.596543 \cdot 10^2\,\text{Å}$, $\alpha_1 = 0.3969775 \cdot 10^{-1}\,\text{Å}^{-1}$, and $\alpha_2 = 5.344506 \cdot 10^2\,\text{Å}^{-1}$.

The embedding energy is

$$F(\bar\rho) = F_0 + \frac{1}{2}F_2(\bar\rho - 1)^2 + q_0(\bar\rho - 1)^3 + \sum_{i=1}^{3} B_i(\bar\rho - 1)^{i+3}\,, \tag{6}$$

where $\bar\rho$ is the host electron density divided by its value at equilibrium. The values of the parameters B_i are $B_1 = 1.549707$, $B_2 = -0.4471131$, and $B_3 = 0.8594003 \cdot 10^{-1}$. The parameters F_0 and F_2 are respectively the embedding energy and its second derivative at equilibrium and the parameter q_0 is chosen such that $F(0) = 0$; for their determination see Ref.[26]. In this work, the embedding energy, electron density and pair potential were used in the tabular form, as provided by the Interatomic Potentials Repository of the National Institute of Standards and Technology[27].

The EAM model, proposed by Zope and Mishin, has been modified in Ref.[28] by a simple scaling of the potential energy of a particle i. This leads to the energy $\tilde U_i = \lambda U_i$ where the parameter λ has been optimized with respect to the temperature dependence of self-diffusion coefficient of Ti melts around T_{m}, as measured by quasi-elastic neutron scattering. With the choice $\lambda = 1.245$ almost perfect agreement with the experimental data for the self-diffusion coefficient is obtained and also the melting temperature T_{m} of this modified EAM model is in better agreement with experiment than the original Zope-Mishin model (see below). In the following, we refer to the modified interaction model of Ti as ModZoM.

III. DENSITY OF THE BULK PHASES

Properties of the liquid and crystalline bcc bulk phases were estimated from simulations in a cubic simulation box using periodic boundary conditions. In these simulations, the velocity Verlet algorithm[29] was used with an integration time step of 1.018 fs. As a first step, we study the dependence of mass density $\rho = Nm_{\mathrm{Ti}}/V$ (with m_{Ti} the mass of Ti and V the volume) and other properties such as the distributions of local order parameters (see below) on the temperature T. To this end, we heated up crystals starting from bcc configurations at low temperature, while the liquids were cooled down starting from equilibrated melt configurations at 2200 K (well above the melting temperature T_{m}). The simulations were performed along the isobare at zero pressure, $p = 0$, by varying the temperature. At each temperature the following sequence of steps was performed; first the system is equilibrated in the NpT ensemble, then the mean density $\langle\rho\rangle$ is determined in another NpT simulation and the instantaneous particle coordinates and box lengths at the end of this run were scaled by the factor $(\langle\rho\rangle/\rho)^{-1/3}$ to match the mean density. In the last step, the properties were estimated in an NVT production run. A stochastic thermostat, where particle velocities are drawn from a Maxwell-Boltzmann distribution every 1200

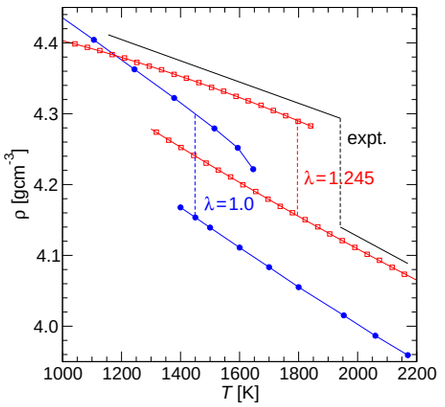

FIG. 1. a) Density $\rho(T)$ of the Zope-Mishin (blue lines) and the ModZoM (red lines) potentials of Ti in comparison to experimental data[30] (black lines).

time steps, and the Berendsen barostat were used to control the temperature and pressure[29].

The results for the density of the bulk crystalline bcc and liquid phases in comparison to experimental data are shown in Fig. 1. The simulation data is well described by the quadratic form

$$\rho(T) = a + b\cdot(T - T_m) + c\cdot(T - T_m)^2\,, \qquad (7)$$

where a, b, and c are fit parameters. We set $T_m = 1796\,\mathrm{K}$, which corresponds to the melting temperature of the ModZoM model (see below).

For the bcc phase, we obtain $a = 4.29036\,\mathrm{g\,cm^{-3}}$, $b = -1.73322\cdot10^{-4}\,\mathrm{g\,cm^{-3}K^{-1}}$ and $c = -3.97396\cdot10^{-8}\,\mathrm{g\,cm^{-3}K^{-2}}$. These values were determined in the range $1000\,\mathrm{K} \le T \le T_\mathrm{m}$. For the bulk liquid phase, we find $a = 4.15596\,\mathrm{g\,cm^{-3}}$, $b = -2.34886\cdot10^{-4}\,\mathrm{g\,cm^{-3}K^{-1}}$ and $c = 2.41224\cdot10^{-8}\,\mathrm{g\,cm^{-3}K^{-2}}$. These values are determined in the range $1300\,\mathrm{K} \le T \le 2200\,\mathrm{K}$, i.e. data points corresponding to the undercooled liquid are included in the fit procedure. Note that close to the melting temperature the density of both the crystalline and melt phases of the ModZoM exhibit a much better agreement with experiment than the original model of Zope and Mishin.

The specific latent heat $\tilde{H}_s(T,p) - \tilde{H}_l(T,p)$ is given by

$$\Delta\tilde{H}(T) = A + B\cdot(T - T_m) + C\cdot(T - T_m)^2 \qquad (8)$$

with $A = 2.71984\cdot10^5\,\mathrm{J\,kg^{-1}}$, $B = 43.5394\,\mathrm{J\,kg^{-1}K^{-1}}$ and $C = -0.0691188\,\mathrm{J\,kg^{-1}K^{-2}}$. These values are fitted using the data in the temperature range $1400\,\mathrm{K} \le T \le T_\mathrm{m}$. Part of the metastable phases is included in the fit procedure. At the melting temperature, the mass density of the solid is $\rho_s = 4.29036\,\mathrm{g\,cm^{-3}}$, that of the liquid $\rho_l = 4.15596\,\mathrm{g\,cm^{-3}}$, and the latent heat $\Delta\tilde{H}_\mathrm{m} = 2.71984\cdot10^2\,\mathrm{J\,g^{-1}}$. Note that the experimental value is $\Delta\tilde{H}_\mathrm{m} = 2.95\cdot10^2\,\mathrm{J\,g^{-1}}$ (thus, the value predicted by the ModZoM model is in good agreement with the experimental value).

The specific heat capacity of the bcc and liquid phases are well described by

$$\tilde{c}_s(T) = \tilde{A} + \tilde{B}\cdot(T - T_m)\,. \qquad (9)$$

Here, the fitted values are $\tilde{A} = 0.61407\,\mathrm{J\,g^{-1}K^{-1}}$ and $\tilde{B} = -6.84638\cdot10^{-5}\,\mathrm{J\,g^{-1}K^{-2}}$ for the bcc phase, and $\tilde{A} = 0.57053\,\mathrm{J\,g^{-1}K^{-1}}$ and $\tilde{B} = 6.97738\cdot10^{-5}\,\mathrm{J\,g^{-1}K^{-2}}$ for the liquid phase.

IV. MELTING TEMPERATURE AND KINETIC GROWTH COEFFICIENTS

Reliable estimates of the melting temperature and kinetic growth coefficients were obtained by simulation with the free solidification method (FSM)[7,31,32]. In this method, inhomogeneous systems are considered where the crystalline and the liquid phase coexist in elongated simulation box with periodic boundary conditions in the three spatial directions. The two phases are separated by two planar interfaces. Then, MD simulations at constant pressure and temperature are performed. During the simulation the stable phase grows into metastable one. In the steady growth regime, the interfaces move with constant velocity v_I. Under equilibrium conditions, i.e. at T_m, the interface velocity is zero. Thus, one determines v_I as a function of temperature and extrapolates the data to $v_\mathrm{I} = 0$ to get an estimate of the melting temperature T_m.

To prepare the system we used the protocol described in our previous work [33]. First, atoms are arranged in a perfect crystal in an elongated simulation box considering a geometry compatible with the studied crystalline orientation. The crystal is relaxed in a NpT simulation run where the density of the crystalline phase at the prescribed pressure and temperature is determined. As next, two regions are defined in the system; the crystal and the melt. The temperature of the atoms in the melt region is raised above T_m while the atoms in the crystalline solid region are frozen. The temperature of the melt region is chosen as the temperature at which the homogeneous crystalline phase melts in a heating simulation, see Fig. 1. This step is performed in an Np_zAT run where the pressure of the melt region is calculated considering the virial contribution of all pairs that involve the atoms in the melt region, including the interactions between atoms in the melt and atoms in the crystal, and the volume of the melt region. In the next simulation step, the melt is cooled down in a Np_zAT simulation run at the same temperature and pressure chosen to prepare the crystal. In the preparation of the melt the scaling of the z coordinates is applied only in the melt region, otherwise, a strain would be artificially imposed in the crystalline region. In the last step, all the atoms in the system are allowed to participate in the dynamics and the growth of the stable phase occurs. The melting, cooling and growth steps are performed in Np_zAT simulation runs. In these simulations the cross section of the box, A, remains constant while the pressure p_z is controlled using the Berendsen barostat[34], i.e. the box length and the atoms positions in the direction perpendicular to the planar crystal-liquid interfaces, z, are scaled by a factor $1 + \alpha_p(p_z - p_0)$ at each integration step. The barostat coupling parameter α_p was set equal to 10^{-3} [$\mathrm{eV^{-1}\AA^3}$] which corresponds to a rather weak coupling. Using this value no stresses are induced by the crystal growth process, as shown in the results of growth simulations for different crystalline

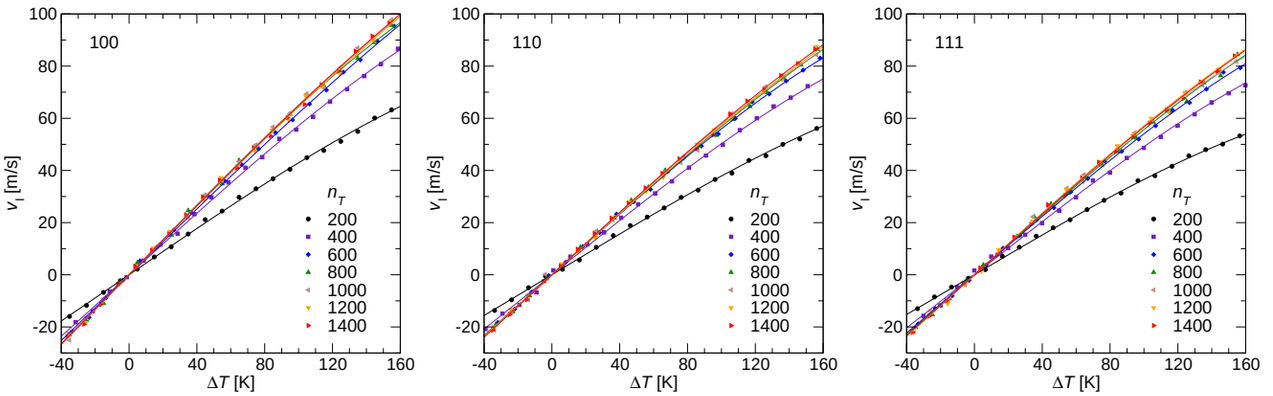

FIG. 2. a) Growth velocity versus undercooling ($\Delta T = T_\mathrm{m} - T$) of the ModZoM model of Ti for the crystalline orientations 100, 110 and 111 at different values of the thermostat coupling parameter (n_T). Solid lines correspond to the polynomial fit of the data from which the kinetic growth coefficient is estimated.

orientations at $T = 1750$ K (supplementary material).
Since the velocity in pure metals is relatively fast ($v_I \approx 10^1$ to 10^2 m/s), growth can be observed in the simulations after some picoseconds. The interfacial growth velocity v_I is related to the rate of change in total volume V by means of the mass balance $m = \rho_\mathrm{I} V_\mathrm{I} + \rho_\mathrm{s} V_\mathrm{s}$ which for $\dot{m} = 0$ and $V = V_\mathrm{I} + V_\mathrm{s}$ leads to

$$v_\mathrm{I} = \frac{\rho_\mathrm{I}}{2A(\rho_\mathrm{s} - \rho_\mathrm{I})} \frac{dV}{dt} \tag{10}$$

where A is the area of the section transversal to the growth direction, ρ_s and ρ_l are the densities of the crystalline and liquid phases, respectively.

Growth velocities for the crystal orientations 100, 110 and 111 of Ti bcc crystals were determined in the temperature range $1640\,\mathrm{K} \leq T \leq 1830\,\mathrm{K}$ in steps of 10 K between successive temperatures. At each temperature, five independent simulation runs were performed to obtain a reliable estimate of the interface velocity. The number of unit cells in each direction of the initial bcc crystal were chosen such that the geometry of the simulation box is $L_x \approx L$, $L_y \approx L$ and $L_z \approx 16L$ with $L \approx 40$ Å. For the initial width of the crystalline region, $L_c \approx L_z/3$ was chosen. The simulations were also done for different values of the thermostat parameter n_T (every n_T steps new velocities from a Maxwell-Boltzmann distribution are generated such that the total momentum of the system is kept constant).

Simulation results for the linear growth velocity at different undercooling for the crystalline orientations 100, 110 and 111 are shown in Figure 2. In each plot, the different curves correspond to different values of the thermostat parameter n_T. Close to coexistence the growth velocity follows the linear relation $v_I(T) = \mu \Delta T$ where $\Delta T = T_\mathrm{m} - T$ is the undercooling and μ the kinetic growth coefficient for a given crystalline orientation. At high undercooling, the dependence of growth velocity on temperature is weaker than expected from extrapolation of the linear behaviour at coexistence $\Delta T = 0$. For the temperature interval considered, the dependence of v_I on ΔT

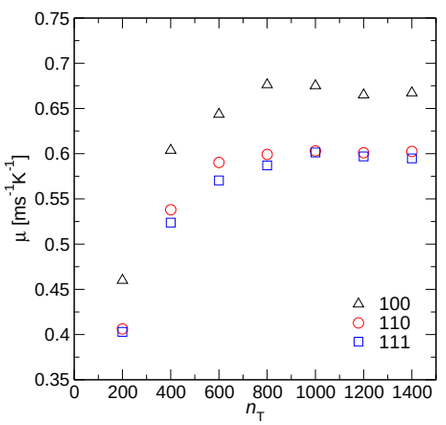

FIG. 3. Kinetic growth coefficients for the crystalline orientations 100, 110 and 111 for different values of the thermostat parameter n_T.

is well described by a cubic polynomial

$$v_\mathrm{I} = \mu \Delta T + c \Delta T^3. \tag{11}$$

The kinetic growth coefficient is obtained as the slope of the data around $\Delta T = 0$.

Figure 2 indicates that for $n_T \geq 1000$ the results for the interface velocity do not seem to be affected by the coupling to the thermostat. The melting temperature that we obtain from our data is $T_\mathrm{m} = 1796 \pm 2$ K, which is in fair agreement to the experimental value $T_m = 1941$ K. Figure 3 shows the estimated kinetic coefficient as a function of the thermostat parameter n_T. As we have already guessed from the behavior of the interface velocity, the values for the different μ's saturate to a constant for $n_T > 1000$. So our estimates of the kinetic growth coefficients for the different crystal orientations are $\mu_{100} = 0.670\,\mathrm{m\,s^{-1}K^{-1}}$, $\mu_{110} = 0.600\,\mathrm{m\,s^{-1}K^{-1}}$ and $\mu_{111} = 0.596\,\mathrm{m\,s^{-1}K^{-1}}$.

TABLE I. Kinetic growth coefficients for different crystalline orientations.

Orientation	μ/μ_0
100	$1+(2/5)\delta_1+(4/7)\delta_2$
110	$1-(1/10)\delta_1-(13/14)\delta_2$
111	$1-(4/15)\delta_1+(64/63)\delta_2$

The orientational dependence of the kinetic coefficient, i.e. the kinetic coefficient as function of the unitary crystal orientation vector $\hat{\mathbf{n}}=(n_1,n_2,n_3)$, can be described in terms of a *cubic harmonics* expansion, as proposed by Fehlner and Vosko[35]

$$\frac{\mu(\hat{\mathbf{n}})}{\mu_0}=1+\delta_1\left(Q-\frac{3}{5}\right)+\delta_2\left(3Q+66S-\frac{17}{7}\right)$$

with $Q=n_1^4+n_2^4+n_3^4$ and $S=n_1^2n_2^2n_3^2$. The parameters in the expansion are μ_0, a sort of orientationally averaged value of the kinetic growth coefficient; δ_1 and δ_2 can be interpreted as dimensionless anisotropy coefficients. Using the MD estimates of μ_{100}, μ_{110} and μ_{111} for our ModZoM model of Ti, the expansion parameters are given by $\mu_0=0.619\,\mathrm{m\,s^{-1}K^{-1}}$, $\delta_1=0.187848$, and $\delta_2=0.0127778$. In comparison to fcc nickel (using the EAM of Foiles[36]), the anisotropy coefficients of the kinetic coefficient are much smaller (for Ni: $\delta_1=1.27707$, $\delta_2=-0.136194$). Note that in both systems $\delta_1>\delta_2$ holds.

V. INTERFACIAL STIFFNESSES AND TENSIONS

Crystal-liquid interfaces in Ti are rough and exhibit thermal undulations that in the limit of long wavelengths are known as capillary waves. These undulations can be described in terms of a height function $h(\mathbf{r})$ that depends on the lateral position $\mathbf{r}=(x,y)$ with respect to the interface. The study of height-height correlations allows to estimate static and dynamic interfacial properties[3,52]. As we shall see below, in a crystal-liquid interface, the capillary wave spectrum is anisotropic governed by stiffness coefficients, $\tilde{\gamma}_{z\alpha}$, where$z$ indicates the direction perpendicular to the interface, and α the direction along which the capillary waves propagate, $\alpha=x$ (or y).

According to capillary wave theory (CWT)[41–47], in the long-wavelength limit the free energy of a given realization of the interface height profile, $h(\mathbf{r})$, in the anisotropic interface at coexistence is given by[44,53]

$$\Omega[h(\mathbf{r})]=\int d\mathbf{r}\left[\frac{\tilde{\gamma}_{zx}}{2}\left(\frac{\partial h}{\partial x}\right)^2+\frac{\tilde{\gamma}_{zy}}{2}\left(\frac{\partial h}{\partial y}\right)^2\right]. \tag{12}$$

The free energy functional $\Omega[h(\mathbf{r})]$ can be understood as an effective CWT Hamiltonian. By writing $h(\mathbf{r})$ in terms of Fourier modes, $h(\mathbf{r})=\sum h_{\mathbf{q}}e^{i\mathbf{q}\cdot\mathbf{r}}$, the CWT Hamiltonian can be written as

$$\Omega_{\mathbf{q}}[h]=A\sum\left[\tilde{\gamma}_{zx}q_x^2+\tilde{\gamma}_{zy}q_y^2\right]|h_{\mathbf{q}}|^2 \tag{13}$$

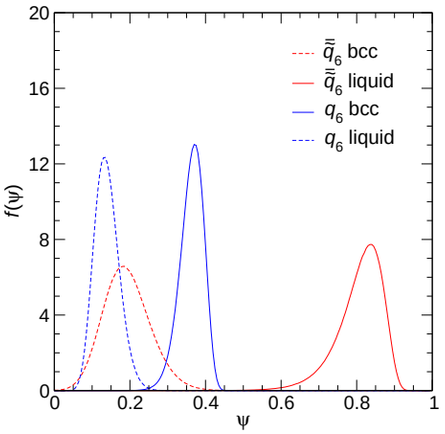

FIG. 4. Distributions of the local order parameter q_6 of Steinhardt *et al.* (blue) and $\tilde{\bar{q}}_6$ of Eslami *et al.* (red) in the bcc crystal phase (solid) and liquid phase (dashed) of Ti at the melting temperature $T_\mathrm{m}=1796$ K.

where A is the area of the interface. The expression for $\Omega_{\mathbf{q}}[h]$ is a quadratic form, so that using the equipartition theorem, we find that the mean squared fluctuations of the interface profile in the long wave limit are given by

$$\langle|h(\mathbf{q})|^2\rangle=\frac{k_BT_\mathrm{m}}{A\left[\tilde{\gamma}_{zx}q_x^2+\tilde{\gamma}_{zy}q_y^2\right]} \tag{14}$$

A. Interfacial height profile

The interfacial height profile $h(\mathbf{r})$ can be computed from the deviations of the interface position $z(x,y)$ with respect to its instantaneous mean value, $h(x,y)=z(x,y)-\langle z(x,y)\rangle$. The interface position $z(x,y)$ is determined by identifying atoms as embedded in a crystalline or liquid local environment using a suitable rotationally invariant local order parameter such as the local bond order parameters $q_l(i)$ introduced by Steinhardt *et al.*[37],

$$q_l(i)=\left(\frac{4\pi}{2l+1}\sum_{m=-l}^{l}|q_{lm}(i)|^2\right)^{1/2} \tag{15}$$

where

$$q_{lm}(i)=\frac{1}{N_b(i)}\sum_{j\in N_b(i)}Y_l^m(\phi_{ij},\varphi_{ij}). \tag{16}$$

In Eqs. (15) and (16), $N_b(i)$ is the number of neighbors of a particle i, $Y_l^m(\phi_{ij},\varphi_{ij})$ are spherical harmonic functions with ϕ_{ij} and φ_{ij} the polar and azimuthal angles of the vector $\hat{\mathbf{r}}_{ij}$. Another local bond order parameter $\hat{q}_l(i)$ was introduced by Eslami *et al.*[38]

$$\tilde{q}_l(i)=\frac{1}{N_b(i)}\sum_{j\in N_b(i)}\sum_{m=-l}^{l}\hat{q}_{lm}(i)\hat{q}_{lm}^*(j) \tag{17}$$

TABLE II. Simulation box lengths of the systems studied for capillary wave analysis.

n|**t**	$L_x \times L_y \times L_z$ Å^3
100[001]	$293.12 \times 26.65 \times 298.10$
110[1$\bar{1}$0]	$301.47 \times 26.65 \times 306.69$
110[001]	$293.12 \times 23.55 \times 306.69$
111[$\bar{1}$10]	$301.47 \times 24.48 \times 281.66$
111[11$\bar{2}$]	$293.70 \times 28.27 \times 281.66$

with

$$\hat{q}_{lm}(i) = \frac{q_{lm}(i)}{\left(\sum_{m=-l}^{l} |q_{lm}(i)|^2\right)^{1/2}} \tag{18}$$

Additionally, as in the work of Lechner and Dellago[39], the order parameter is averaged over neighboring particles including the value at particle i,

$$\bar{\tilde{q}}_l(i) = \frac{1}{1+N_b(i)} \left[\tilde{q}_l(i) + \sum_{j \in N_b(i)} \tilde{q}_l(j) \right]. \tag{19}$$

The distributions of the parameter q_6 of Steinhardt *et al.* and $\bar{\tilde{q}}_6$ of Eslami *et al.* in the bulk liquid and crystal phases of Ti at the melting temperature are shown in Figure 4. For the computation of these order parameters a cut-off radius $r_c = 4.0$ Åwas chosen, which corresponds to the first two shells of neighbors, i.e. the mean coordination number of a particle in the crystal is $N_b \approx 14$.

The distributions of local order parameter in the crystalline and liquid phases are well differentiated, however, the overlapping of modes is lower in the order parameter of Eslami *et al.* (Figure 4).

The determination of the local position of the interface is performed in three steps. In the first step, crystal-like particles are identified as those whose order parameter value is larger than a given threshold. For the order parameter $\bar{\tilde{q}}_6$ this threshold is chosen equal to 0.43, which corresponds to the intersection of the order parameter distributions of the crystalline and liquid phases. In the second step, particles in the bulk of the liquid that are identified as crystal-like particles in the first step are discarded as part of the crystal. For this purpose, the crystal phase is defined as the largest cluster of crystal-like particles. In the last step, the interface is defined as the set of particles at the crystal surface. These particles are identified by the cone algorithm[40]. The procedure is illustrated in Figure 5.

B. Capillary wave spectrum

The simulations were performed in a slab geometry, where the simulation box is much larger in the directions parallel to the interface orientation z and parallel to the tangential direction x (see Table II).

TABLE III. Interfacial tensions for different crystalline orientations.

n	γ/γ_0
100	$1+(2/5)\varepsilon_1+(4/7)\varepsilon_2+(4/13)\varepsilon_3$
110	$1-(1/10)\varepsilon_1-(13/14)\varepsilon_2+(9/52)\varepsilon_3$
111	$1-(4/15)\varepsilon_1+(64/63)\varepsilon_2+(32/351)\varepsilon_3$

The spectrum of capillary wave fluctuations is estimated along the tangential direction x, for which the wave vector $\mathbf{q} = (q_x, 0)$ is replaced in Eq. (14) and the stiffness is determined by extrapolating to the long wave limit $q_x \to 0$

$$\tilde{\gamma}_{zx} = \lim_{q_x \to 0} \frac{k_B T_\mathrm{m}}{A \langle |h(q_x)|^2 \rangle q_x^2} \tag{20}$$

The capillary waves spectrum for the crystalline orientations 100, 110 and 111 along the main tangential directions at zero pressure and $T_\mathrm{m} = 1796$ K are presented in Figure 6. Each curve was obtained from the average of ten independent simulations, where $5 \cdot 10^6$ simulation steps were made in each simulation run. The interfacial stiffnesses are estimated by extrapolation of the data $\tilde{\gamma}$-q_x to the limit $q_x \to 0$, where the value of the lowest wave number is not considered since the equilibration time of this mode is much larger than the others. The results are $\tilde{\gamma}_{100[001]} = 0.10037\,\mathrm{J\,m^{-2}}$, $\tilde{\gamma}_{110[1\bar{1}0]} = 0.15423\,\mathrm{J\,m^{-2}}$, $\tilde{\gamma}_{110[001]} = 0.11466\,\mathrm{J\,m^{-2}}$, $\tilde{\gamma}_{111[\bar{1}10]} = 0.13427\,\mathrm{J\,m^{-2}}$, and $\tilde{\gamma}_{111[11\bar{2}]} = 0.13487\,\mathrm{J\,m^{-2}}$.

The orientational dependence of the interfacial free energy can be described by the *cubic harmonics* expansion[35]

$$\frac{\gamma(\hat{\mathbf{n}})}{\gamma_0} = 1 + \varepsilon_1 \left(Q - \frac{3}{5} \right) + \varepsilon_2 \left(3Q + 66S - \frac{17}{7} \right) + \varepsilon_3 \left(5Q^2 - 16S - \frac{94}{13} Q + \frac{33}{13} \right) \tag{21}$$

where Q and S are defined in terms of the components of the unitary crystal orientation vector $\hat{\mathbf{n}}$. The expressions of the interfacial tensions for the orientations 100, 110 and 111 are given in Table III.

Expressions for the interfacial stiffnesses can be deduced by replacing $\hat{\mathbf{n}}$ by $\cos\theta\hat{\mathbf{n}} + \sin\theta\hat{\mathbf{t}}$ in the cubic expansion, then using the relation between the stiffness and interfacial tension, $\tilde{\gamma} = \gamma + \partial^2\gamma/\partial\theta^2$, and taking the limit $\theta \to 0$. Expressions of the stiffness for different orientations and tangential directions are summarized in Table IV.

Using the values of the stiffnesses obtained from MD simulations in the corresponding expression of Table IV, the parameters of the cubic harmonics expansion, Eq. (21), are $\gamma_0 = 0.121301\,\mathrm{J\,m^{-2}}$, $\varepsilon_1 = 0.0550041$, $\varepsilon_2 = 0.00178142$ and $\varepsilon_3 = -0.00425494$. With these parameter values the interfacial tensions according to Eq. (21) are $\gamma_{100} = 0.123934\,\mathrm{J\,m^{-2}}$, $\gamma_{110} = 0.120343\,\mathrm{J\,m^{-2}}$, and $\gamma_{111} = 0.119694\,\mathrm{J\,m^{-2}}$. Although the tension values are very similar they follow $\gamma_{100} > \gamma_{110} > \gamma_{111}$ in agreement with the bcc-liquid interface of the Yukawa potential[17]. The interfacial free energy expressed in units of

(a) (b) (c)

FIG. 5. The crystal-liquid interface position (at the top) is identified in three steps: (a) the particles are identified as crystal-like (red) if the local order parameter is larger than a threshold, (b) the crystal is defined as the largest cluster of crystal-like particles, (c) the crystal (top) surface is the collection of particles that have no neighbors on the direction $+z$ on a small area xy centered at their positions.

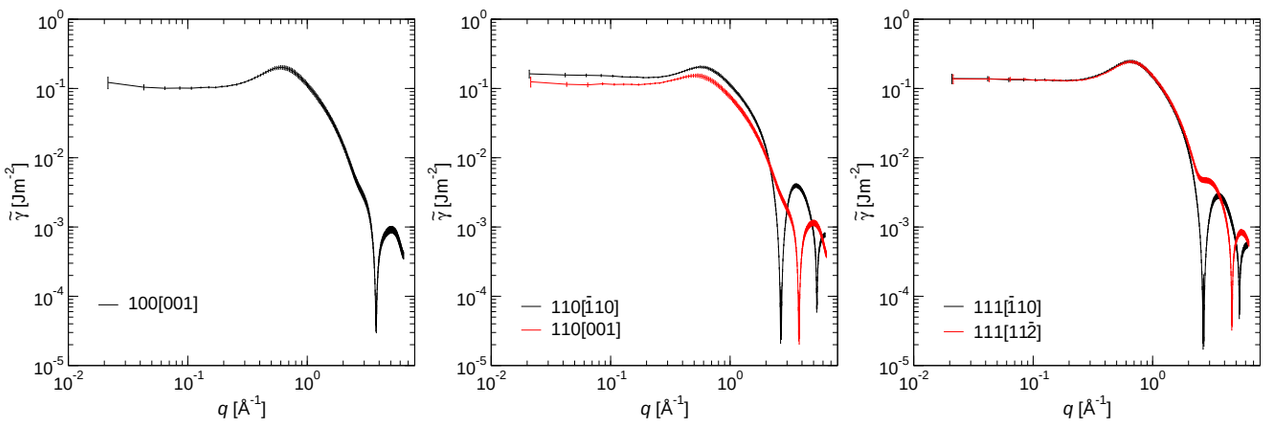

FIG. 6. Capillary wave spectra of the ModZoM model of Ti for the crystalline orientations 100[001], 110[1$\bar{1}$0], 110[001], 111[$\bar{1}$10] and 111[11$\bar{2}$].

TABLE IV. Interfacial stiffnesses for different crystalline orientations and tangential directions.

n|**t**	$\tilde{\gamma}/\gamma_0$
100[010];	
100[001]	$1-(18/5)\varepsilon_1-(80/7)\varepsilon_2-(140/13)\varepsilon_3$
110[1$\bar{1}$0];	$1+(39/10)\varepsilon_1+(155/14)\varepsilon_2-(35/4)\varepsilon_3$
110[001]	$1-(21/10)\varepsilon_1+(365/14)\varepsilon_2-(175/52)\varepsilon_3$
111[$\bar{1}$10];	
111[11$\bar{2}$]	$1+(12/5)\varepsilon_1-(1280/63)\varepsilon_2-(1120/351)\varepsilon_3$

$\Delta\bar{H}_m\sigma^{-2}$, with $\Delta\bar{H}_m$ the latent heat per particle and σ the particle diameter estimated from the density number of the crystalline phase $\sigma=\rho_s^{-1/3}$), is known as Turnbull parameter. Turnbull found that this value is 0.45 for many close-packed metals and somewhat lower for other systems[48]. Using the simulation data of this study it is 0.39174 for the ModZoM model of Ti. It is known from simulations that the fcc-liquid interface of the hard spheres model has a orientational averaged value about 0.5[49]. Recently, the capillary wave spectrum of the bcc-liquid interface of charged colloids was determined in experiments. Here, the obtained Turnbull parameter values are 0.58 for the 100 and 0.68 for the 114 orientation[50]. According to Table III, the relative difference between the maximum and minimum values of the interfacial free energy is

$$\frac{\gamma_{100}-\gamma_{111}}{\gamma_0}=\frac{2}{3}\varepsilon_1-\frac{4}{9}\varepsilon_2+\frac{76}{351}\varepsilon_3. \qquad (22)$$

For bcc Ti this difference is 0.0349564, lower than for fcc Ni where $(\gamma_{100}-\gamma_{111})/\gamma_0=0.07043$ (using $\varepsilon_1=0.10191$, $\varepsilon_2=-0.00134$, $\varepsilon_3=0.00876$).

VI. KINETIC COEFFICIENTS FROM CAPILLARY FLUCTUATIONS

Using the theory developed by Karma[51,52], the kinetic growth coefficients can be estimated from the analysis of cap-

illary waves fluctuations. The capillary wave free energy of the the anisotropic interface off-coexistence is given by[44,53]

$$\Omega = \int d\mathbf{r} \left[\frac{\tilde{\gamma}_{zx}}{2} \left(\frac{\partial h}{\partial x} \right)^2 + \frac{\tilde{\gamma}_{zy}}{2} \left(\frac{\partial h}{\partial y} \right)^2 - \Delta p\, h \right] \tag{23}$$

where the pressure difference between the solid and liquid phases, Δp, is included to account the bulk free energy penalty of the liquid phase off-coexistence. For deviations from the melting line by changing temperature instead of pressure, the Clausius-Clapeyron equation relates the pressure difference with the undercooling as

$$\Delta p = \frac{\rho_s \Delta \tilde{H}_m}{T_m} \Delta T. \tag{24}$$

Off coexistence, Δp is finite, and the interface evolves so as to eliminate the unfavorable bulk phase. However, for small deviations away from coexistence the system evolves smoothly according to free energy gradients. The time evolution of $h(\mathbf{r},t)$ can be described by[54]

$$\frac{\partial h(\mathbf{r},t)}{\partial t} = -k \frac{\partial \Omega[h]}{\partial h} \tag{25}$$

where k is a rate constant. Upon evaluation of the functional derivative, this ansatz for the gradient-driven dynamics of the interface yields the following partial differential equation

$$\frac{\partial h(\mathbf{r},t)}{\partial t} = -k \left[\tilde{\gamma}_{zx} \frac{\partial^2 h}{\partial x^2} + \tilde{\gamma}_{zy} \frac{\partial^2 h}{\partial y^2} - \Delta p \right]. \tag{26}$$

Now we seek for the evolving interface solutions of the form $h(\mathbf{r},t) = \sum h_{\mathbf{q}}(t) e^{i\mathbf{q}\cdot\mathbf{r}}$. Plugging this ansatz into Eq. (26) leads to the following equation for the Fourier transform of the height function, $h_{\mathbf{q}}(t)$,

$$\frac{\partial h_{\mathbf{q}}(t)}{\partial t} = -k \left[(\tilde{\gamma}_{zx} q_x^2 + \tilde{\gamma}_{zy} q_y^2)\, h_{\mathbf{q}}(t) - \Delta p\, \delta(\mathbf{q}) \right] \tag{27}$$

From this equation, we obtain the average growth rate of the interface, v_I in the long-wavelength limit as

$$v_I = \frac{\partial h(t)}{\partial t}\Big|_{\mathbf{q}\to 0} = k \Delta p\,. \tag{28}$$

So with Eq. (24) the kinetic growth coefficient is given by

$$\mu = \frac{k \rho_s \Delta \tilde{H}_m}{T_m}. \tag{29}$$

At finite wave-vectors, Eq. (27) provides a first order linear differential equation which is readily solved, yielding

$$h_{\mathbf{q}}(t) = h_{\mathbf{q}}(0) \exp(-t/\tau_{\mathbf{q}}) \tag{30}$$

with the correlation time, $\tau_{\mathbf{q}}$, identified as

$$\frac{1}{\tau_{\mathbf{q}}} = \frac{T_m \mu}{\rho_s \Delta \tilde{H}_m} (\tilde{\gamma}_{zx} q_x^2 + \tilde{\gamma}_{zy} q_y^2)\,. \tag{31}$$

By use of Eq. (30), upon thermal averaging, the following expression is found for the self-correlation function $f_{\mathbf{q}}(t) = \langle h_{\mathbf{q}}(0) h_{\mathbf{q}}(t) \rangle$,

$$f_{\mathbf{q}}(t) = |h(\mathbf{q})|^2 \exp(-t/\tau_{\mathbf{q}}) \tag{32}$$

A fit of the correlation functions obtained from simulation provides the relaxation time $\tau_{\mathbf{q}}$, which can be used to obtain the kinetic growth coefficient[52]. Particularly, by studying fluctuations along either $\alpha = x$ or $\alpha = y$, we find that $1/\tau_{q\alpha} = \frac{T_m \mu \tilde{\gamma}_\alpha}{\rho_s \Delta \tilde{H}_m} q_\alpha^2$. Accordingly, the slope of $1/\tau_{q\alpha}$ yields right away the kinetic growth coefficient μ [15,51,52].

The dynamics embodied in Eq. (32) only accounts for the slow crystal growth mode and thermal capillary wave excitations. Other fast modes, such as lattice vibrations and elastic deformations are not accounted in this expression. Therefore, the self-correlation function can exhibit more than one relaxation[55].

In a study of Karma's relation, Eq. (31), Benet *et al.*[15] determined the self-correlation function $f_{\mathbf{q}}$ for different systems including hard spheres, Lennard Jones centers and TIP4P/2005 water molecules and found that the decay of this function is much better described by a double exponential function

$$f_q(t) = A \exp(-t/\tau_s) + (1-A) \exp(-t/\tau_f) \tag{33}$$

where two characteristic times can be identified. The kinetic growth coefficient was related with the slow mode characteristic time in Eq. (33), τ_s.

In this study we determined the normalized self-correlation function of h_q given by

$$f_{\mathbf{q}}(t) = \frac{\langle h_{\mathbf{q}}(0) h_{\mathbf{q}}(t)^* \rangle}{\langle h_{\mathbf{q}}(0) h_{\mathbf{q}}(0)^* \rangle} \tag{34}$$

where the brackets denote averages over different independent simulations and time origins. The same series of simulations to estimate the interfacial stiffnesses were used. The results of the self-correlation functions for the different crystal-liquid interfaces are shown in Figure 7. Each curve corresponds to an average of 10 independent simulations each with $5 \cdot 10^6$ steps, for each run, 5000 time origins separated by 10^4 time steps were considered. The function h_q was computed as the discrete Fourier transform of the capillary wave fluctuations with h_q the discrete Fourier transform of

$$h_{\mathbf{q}} = \sum_j h(\mathbf{r}_j) \exp(i\mathbf{q}\cdot\mathbf{r}_j) \tag{35}$$

As observed in the Figure. 7 the time dependence of the self-correlation function f_q is well described by a double exponential function for all crystalline orientations and wave numbers considered.

Figure 8 shows that the inverse of the slow characteristic time τ_s exhibits a linear dependence with the square of the wave-number in the long-wavelength limit ($q \to 0$) covered by the simulation. The figure also indicates that all the regressions tend approximately to zero for $q = 0$. The slope of these curves for each orientation together with the corresponding

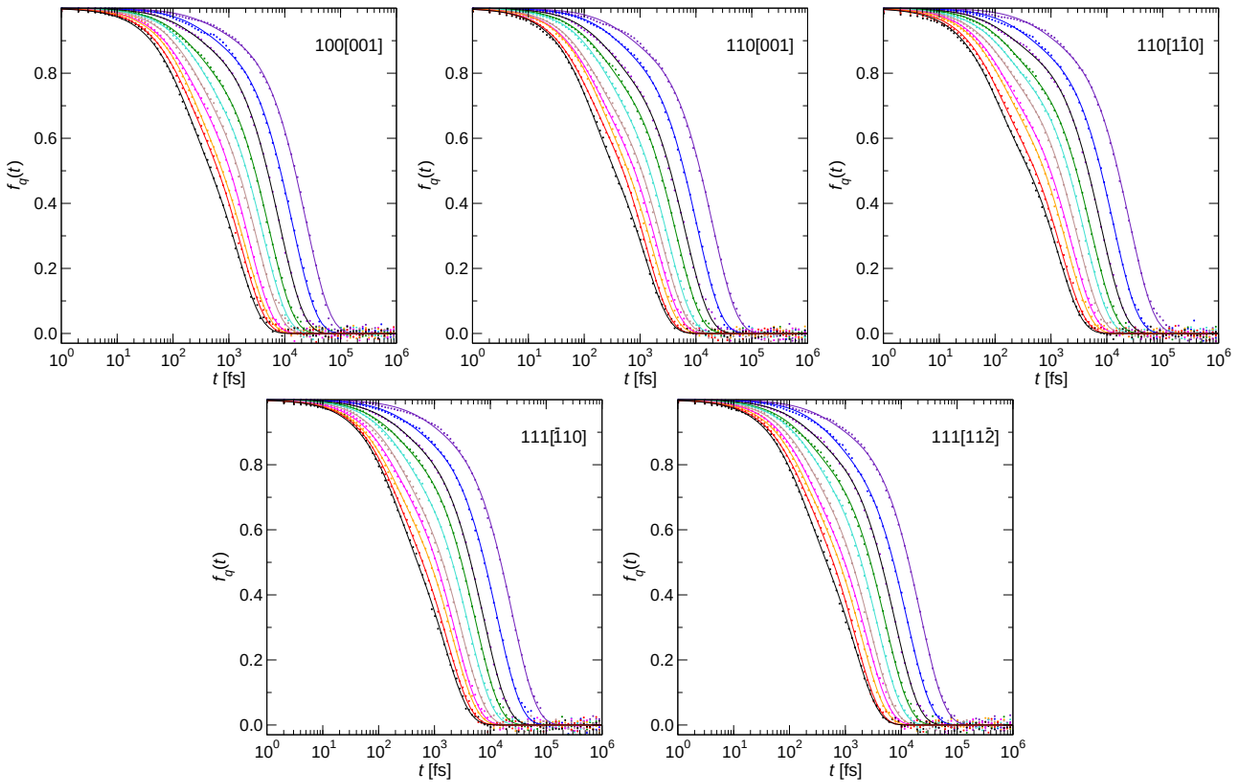

FIG. 7. Self-correlation functions of Ti for the crystalline orientations 100[010], 100[001], 110[1$\bar{1}$0], 110[001], 111[$\bar{1}$10] and 111[11$\bar{2}$]. Curves from right to left correspond to wave-numbers $q = 2\pi n/L_x$ with n from 3 to 13. The fits to double exponential function are shown in solid lines.

TABLE V. Slope of the curves $1/\tau_s$ versus q^2 (Fig. 8) and corresponding kinetic growth coefficients, as estimated from Eq. (31) for different crystalline orientations.

n|**t**	slope [Å^2 ps^{-1}]	μ [ms^{-1}K^{-1}]
100[010];	11.573	0.749
100[001]	-	-
110[1$\bar{1}$0];	14.372	0.605
110[001]	11.824	0.670
111[$\bar{1}$10];	11.938	0.578
111[11$\bar{2}$]	11.591	0.558

kinetic growth coefficient values obtained from Eq. (31) are presented in Table V. The kinetic growth coefficients are in fair agreement with the values obtained from the growth simulations, presented above. The values observed follow the trend $\mu_{100} > \mu_{110} > \mu_{111}$. Using Eq. (31) two different values of μ are obtained for the crystalline orientation 110 (one for each tangential direction). For the orientation 111 this difference is also observed but is not as pronounced as for 110, and corresponds to the small difference in the slopes of the curves $1/\tau_s$ versus q^2 (Fig 8).

VII. SUMMARY AND CONCLUSIONS

We have investigated the crystal growth kinetics of bcc Ti from the melt as well as stiffnesses and free energies of the corresponding crystal-liquid interfaces in Ti. To this end, we have performed molecular dynamics (MD) computer simulations at zero pressure around the melting temperature T_m, using an EAM potential to model the interactions between the Ti atoms. The focus was on the analysis of capillary wave fluctuations, from which we extracted interfacial stiffnesses and free energies as well as kinetic growth coefficients.

We have determined the interfacial stiffness for different crystal orientations. From this information, we have determined the expansion of the stiffness in terms of cubic harmonics, from which we have obtained the interfacial free energy and its anisotropy. For the resulting average interfacial free energy, we have found the value $0.121\,\mathrm{J\,m^{-2}}$, corresponding to a Turnbull parameter of the order of 0.39 which is significantly lower than the typical value for closed-packed structures such as hcp or fcc (e.g. the Turnbull parameter is about 0.5 for fcc hard-sphere crystals). Even "more dramatic" is the effect with respect to the anisotropy of the interfacial free energy. This property is about an order of magnitude smaller for bcc Ti than that for typical fcc systems.

The growth velocities are found to depend significantly on

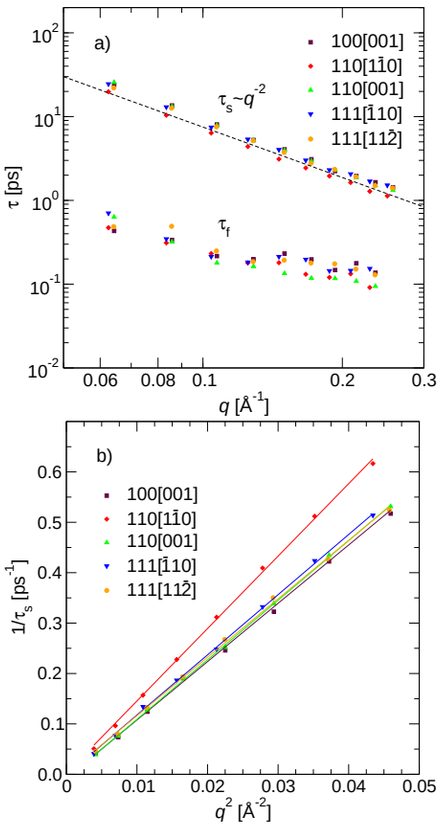

FIG. 8. a) Characteristic times of the slow, τ_s, and fast, τ_f, modes of the self-correlation function f_q versus wave number q for different crystalline orientations. b) Inverse of the slow characteristic time τ_s versus wavenumber squared q^2.

the coupling constant of the thermostat, but converged values are obtained in the limit of a sufficiently weak coupling of the system to the thermostat. Kinetic growth coefficients may be calculated from the slope of the growth velocity at coexistence. Our results show that the growth coefficient of the principal facets of titanium have an average value of $0.619\,\mathrm{m\,s^{-1}\ K^{-1}}$, and again a rather small anisotropy. We have also obtained the kinetic growth coefficients from an analysis of the relaxation dynamics of capillary wave fluctuations. We find that a model with two exponential functions, as proposed by Benet *et al.*[15], fits the self-correlation functions very well and leads to accurate estimates of kinetic growth coefficients from equilibrium fluctuations, in very good agreement with those determined via FSM. The estimate of growth coefficients via the equilibrium capillary wave fluctuations is especially well suited for binary alloys where the FSM method is hardly accessible due to the presence of concentration gradients as well as the formation of defects[16] under non-equilibrium conditions. The use of the capillary fluctuation method for binary alloys to estimate kinetic growth coefficients shall be a theme of forthcoming studies.

SUPPLEMENTARY MATERIAL

See supplementary material for the evolution of the stress tensor components and simulation box length L_z during growth simulations at $T = 1750$ K.

ACKNOWLEDGMENTS

R. E. Rozas acknowledges financial support from Project ANID FONDECYT 1190101. P. G. Toledo and R. E. Rozas acknowledge financial support from Centro CRHIAM Project ANID/FONDAP/15130015.

DATA AVAILABILITY

The data that support the findings of this study are available from the corresponding author upon reasonable request.

[1] J. S. Langer, Rev. Mod. Phys. **52**, 1 (1980).
[2] J. Bragard, A. Karma, Y. H. Lee, and M. Plapp, Interface Sci. **10**, 121 (2002).
[3] J. J. Hoyt, M. Asta, and A. Karma, Phys. Rev. Lett. **86**, 5530 (2001).
[4] J. R. Morris, Phys. Rev. B **66**, 144104 (2002).
[5] R. L. Davidchack, J. R. Morris, and B. B. Laird, J. Chem. Phys. **125**, 094710 (2006).
[6] M. Amini and B. B. Laird, Phys. Rev. Lett. **97**, 216102 (2006).
[7] T. Zykova-Timan, R. E. Rozas, J. Horbach, and K. Binder, J. Phys.: Condens. Matter **21**, 464102 (2009).
[8] R. E. Rozas and J. Horbach, EPL **93**, 26006 (2011).
[9] A. Härtel, M. Oettel, R. E. Rozas, S. U. Egelhaaf, J. Horbach, and H. Löwen, Phys. Rev. Lett. **108**, 226101 (2012).
[10] R. Benjamin and J. Horbach, J. Chem. Phys. **141**, 044715 (2014).
[11] R. Benjamin and J. Horbach, Phys. Rev. E **91**, 032410 (2015).
[12] R. Benjamin and J. Horbach, J. Chem. Phys. **143**, 014702 (2014).
[13] F. Turci and T. Schilling, J. Chem. Phys. **141**, 054706 (2014).
[14] M. Bültmann and T. Schilling, Phys. Rev. E **102**, 042123 (2020).
[15] J. Benet, L. G. MacDowell, and E. Sanz, J. Chem. Phys. **141**, 034701 (2014).
[16] P. Kuhn and J. Horbach, Phys. Rev. B **87**, 014105 (2013).
[17] V. Heinonen, A. Mijailović, C. V. Achim, T. Ala-Nissila, R. E. Rozas, J. Horbach, and H. Löwen, J. Chem. Phys. **138**, 044705 (2013).
[18] D. Y. Sun, M. Asta, and J. J. Hoyt, Phys. Rev. B **69**, 174103 (2004).
[19] Y. F. Gao, Y. Yang, D. Y. Sun, M. Asta, and J. J. Hoyt, J. Cryst. Growth **312**, 3238 (2010).
[20] J. Persson, C. Desgranges, and J. Delhommelle, Chem. Phys. Lett. **511**, 57 (2011).
[21] R. Li, Y. Wu, and J. Xiao, J. Chem. Phys. **140**, 034503 (2014)
[22] L. Wu, H. Wang, Y. Zhu, M. Li, Materialia **15**, 100962 (2021).
[23] D. V. Louzguine-Luzgin and A. I. Bazlov, Metals **10**, 1532 (2020).
[24] J. J. Hoyt, M. Asta, and D. Y. Sun, Philos. Mag. **86**, 3651 (2006).
[25] J. Monk, Y. Yang, M. I. Mendelev, M. Asta, J. J. Hoyt, and D. Y. Sun, Modell. Simul. Mater. Sci. Eng. **18**, 015004 (2010).
[26] R. Zope and Y. Mishin, Phys. Rev. B **68**, 024102 (2003).
[27] See https://www.ctcms.nist.gov/potentials/system/Ti/.
[28] J. Horbach J., R. E. Rozas, T. Unruh, and A. Meyer, Phys. Rev. B **80**, 212203 (2009).
[29] D. Frenkel and B. Smit, *Understanding Molecular Simulation: From Algorithms to Applications* (Academic Press, San Diego, 2002).
[30] K. C. Mills, *Recommended values of thermophysical properties for selected commercial alloys* (Woodhead Publishing, Cambridge, UK, 2002).
[31] J. Q. Broughton, G. H. Gilmer, and K. A. Jackson, Phys. Rev. Lett. **49**, 1496 (1982).
[32] D. Y. Sun, M. Asta, and J. J. Hoyt, Phys. Rev. B **69**, 024108 (2004).

[33]R. E. Rozas, A. D. Demirağ, P. G. Toledo and J. Horbach, J. Chem. Phys. **145** 064515 (2016).
[34]H. J. C. Berendsen, J. P. M. Postma, W. F. van Gunsteren, A. DiNola, and J. R. Haak, J. Chem. Phys. **81**, 3684 (1984).
[35]W. R. Fehlner and S. H. Vosko, Canadian Journal of Physics **54**, 2159 (1976).
[36]S. M. Foiles, Phys. Rev. B **32**, 3409 (1985).
[37]P. J. Steinhardt, D. R. Nelson, and M. Ronchetti, Phys. Rev. B **28**, 784 (1983)
[38]H. Eslami, P. Sedaghat, and F. Müller-Plathe, Phys. Chem. Chem. Phys. **20**, 27059 (2018)
[39]W. Lechner and C. Dellago, J. Chem. Phys. **129**, 114707 (2008).
[40]Y. Wang, S. Teitel, and C. Dellago, J. Chem. Phys. **122**, 214722 (2005).
[41]F. P. Buff, R. A. Lovett, and F. H. Stillinger F. H., Phys. Rev. Lett. **15**, 621 (1965).
[42]J. D. Weeks, J. Chem. Phys. **67**, 3106 (1997).
[43]M. P. A. Fisher, D. S. Fisher, and J. D. Weeks, Phys. Rev. Lett. 48, 368 (1982).
[44]D. S. Fisher and J. D. Weeks, Phys. Rev. Lett. **50**, 1077 (1983).
[45]D. Bedeaux and J. D. Weeks, J. Chem. Phys. **82**, 972 (1985).
[46]M. P. Gelfand and M. E. Fisher, Physica A **166**, 1 (1990).
[47]K. Binder and M. Müller, Int. J. Mod. Phys. C **11**, 1093 (2000).
[48]D. Turnbull, J. Appl. Phys. 21, 1022 (1950).
[49]B. B. Laird, J. Chem. Phys. **115**, 2887 (2001).
[50]H. Hwang, D. A. Weitz, and F. Spaepen, Proc. Natl. Acad. Sci. U.S.A. **117**, 25225 (2020).
[51]A. Karma, Phys. Rev. E **48**, 3441 (1993).
[52]J. Hoyt, M. Asta, and A. Karma, Interface Sci. **10**, 181 (2002).
[53]N. Akutsu and T. Yamamoto, *Handbook of Crystal Growth (Second Edition)*, (Elsevier, Boston, USA, 2015)
[54]D. Sibley, P. Llombart, E. G. Noya, A. Archer, and L. G. MacDowell, Nat. Commun. **12**, 239 (2021).
[55]M. L. Henle and A. J. Levine, Phys. Rev. E **75**, 021604 (2007).

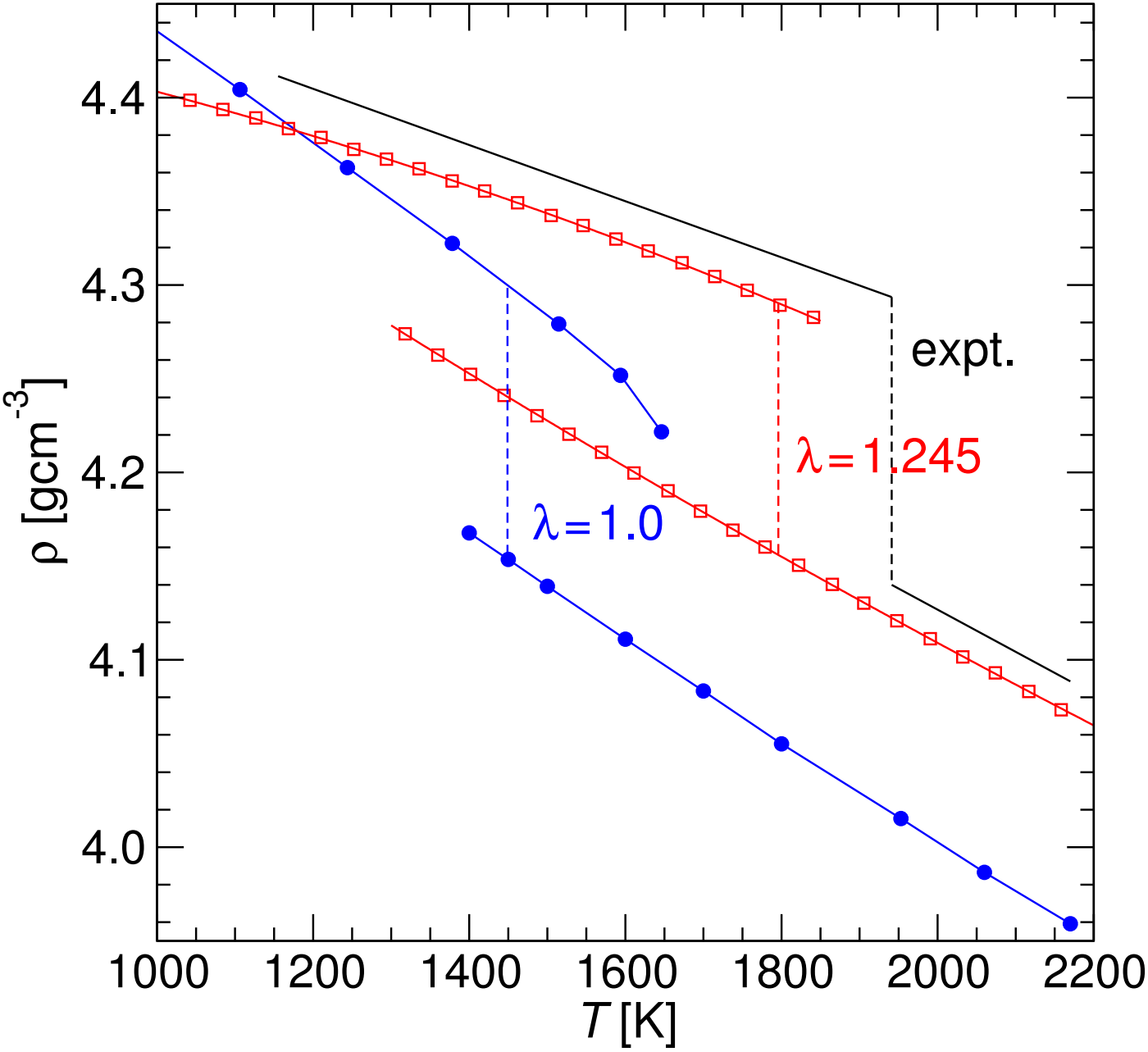
4.4
4.3
4.2
4.1
4.0
ρ [gcm^{-3}]
1000
1200
1400
1600
1800
2000
2200
T [K]
expt.
λ=1.245
λ=1.0

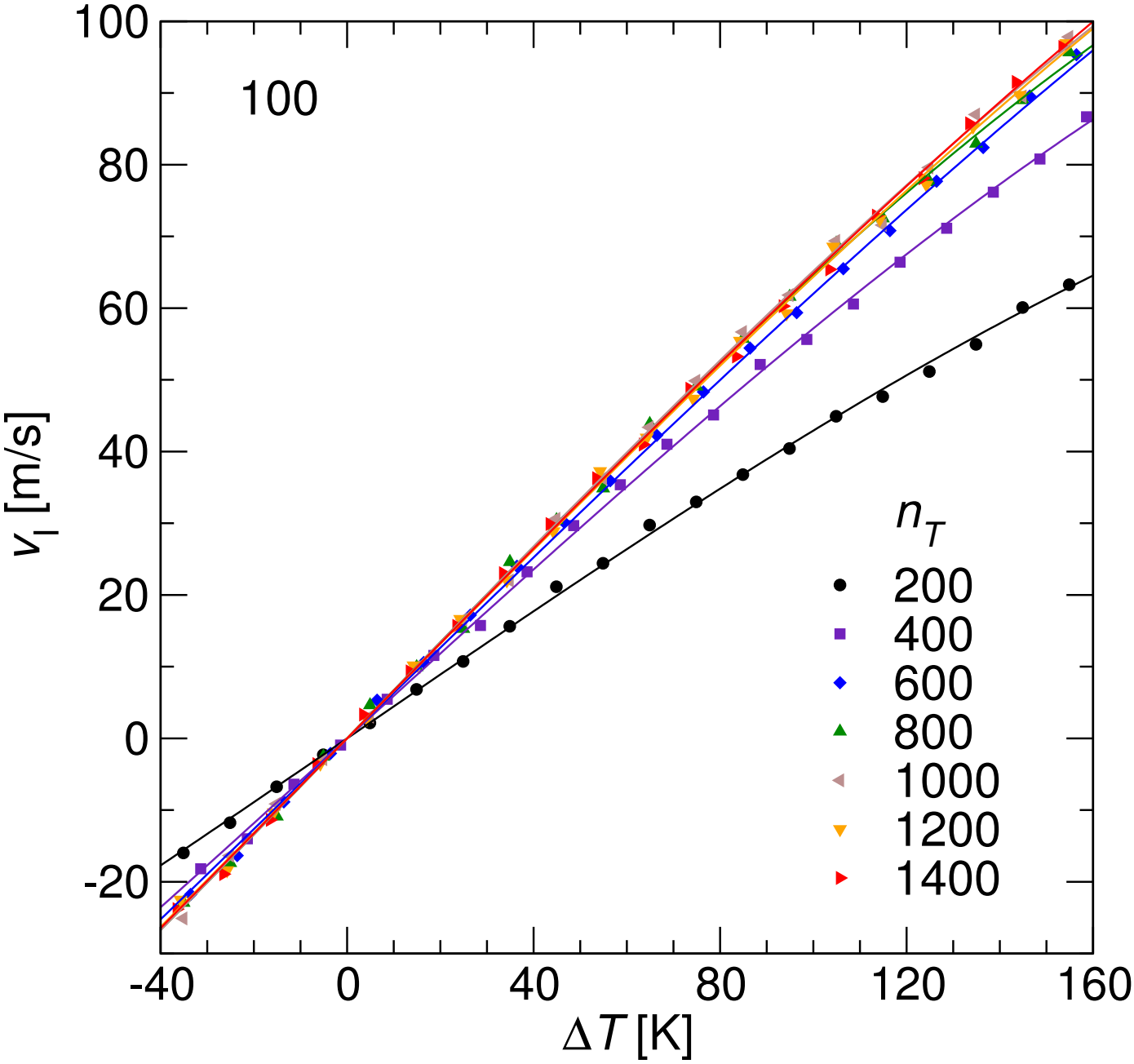
100
v_l [m/s]
ΔT [K]
n_T
200
400
600
800
1000
1200
1400
100
80
60
40
20
0
-20
-40
0
40
80
120
160

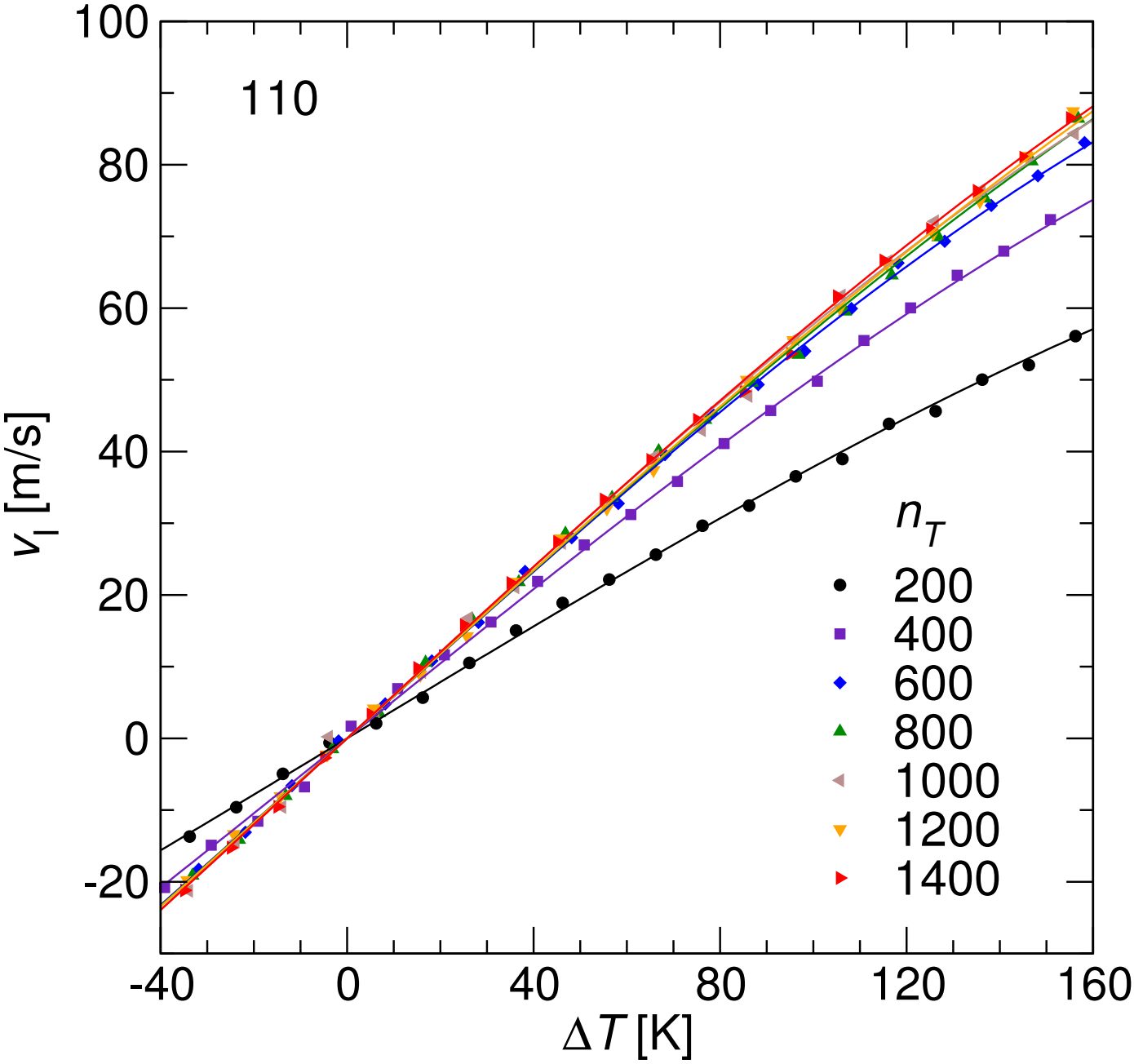
110
v_l [m/s]
ΔT [K]
n_T
200
400
600
800
1000
1200
1400
100
80
60
40
20
0
-20
-40
0
40
80
120
160

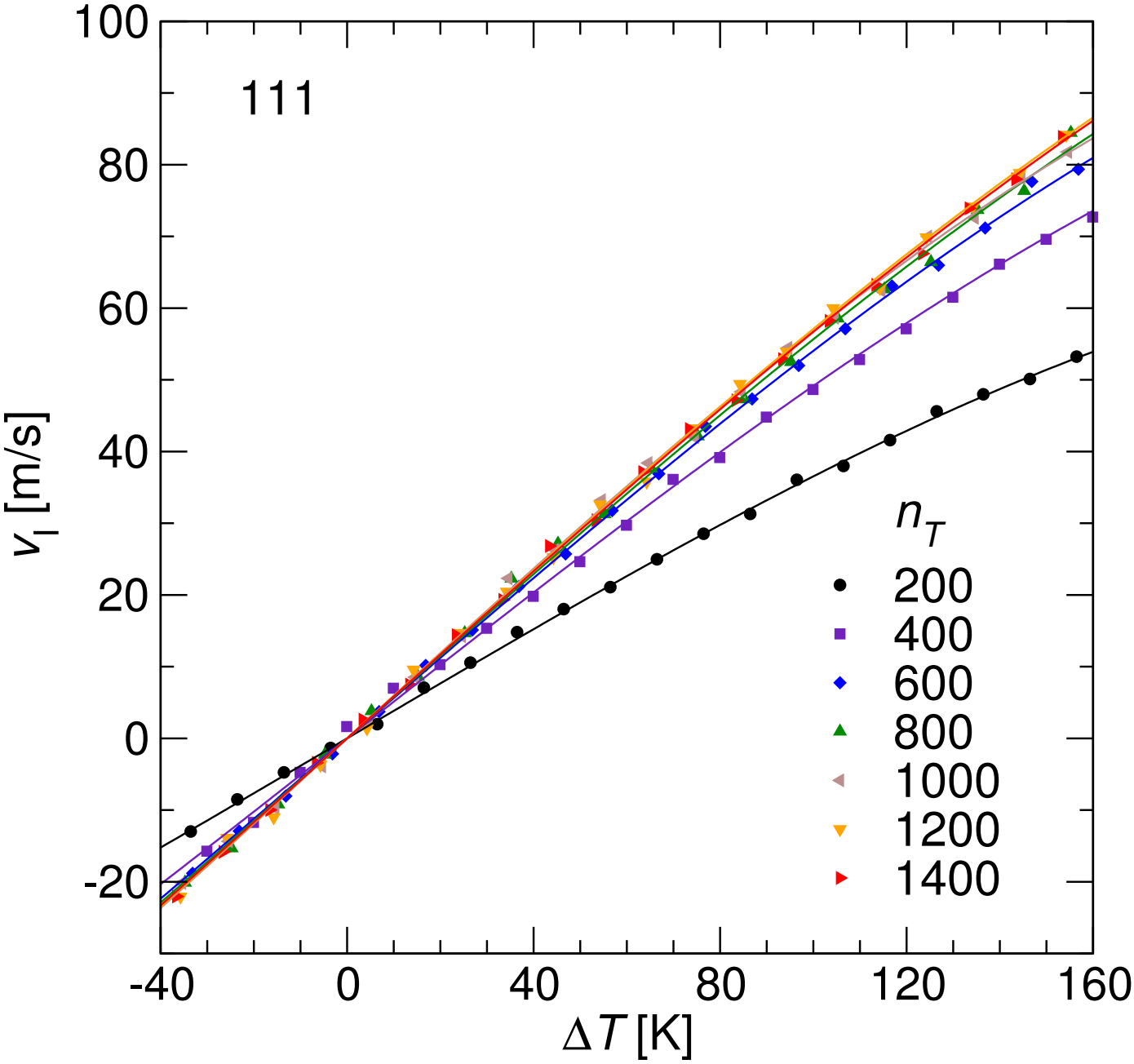
111
v_l [m/s]
ΔT [K]
100
80
60
40
20
0
-20
-40
0
40
80
120
160
n_T
200
400
600
800
1000
1200
1400

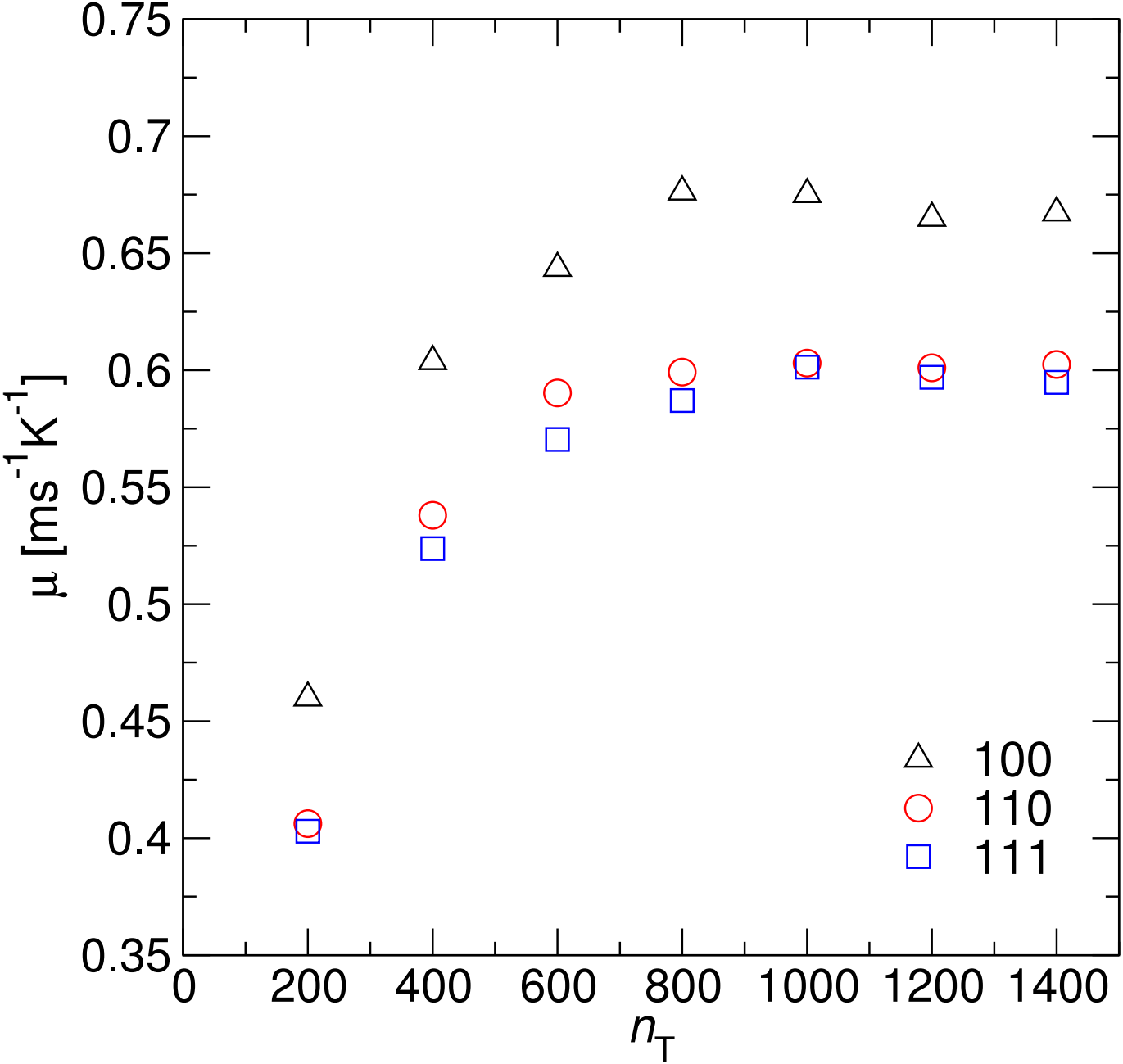
0.75
0.7
0.65
0.6
0.55
0.5
0.45
0.4
0.35
μ [ms^{-1}K^{-1}]
0
200
400
600
800
1000
1200
1400
n_T
100
110
111

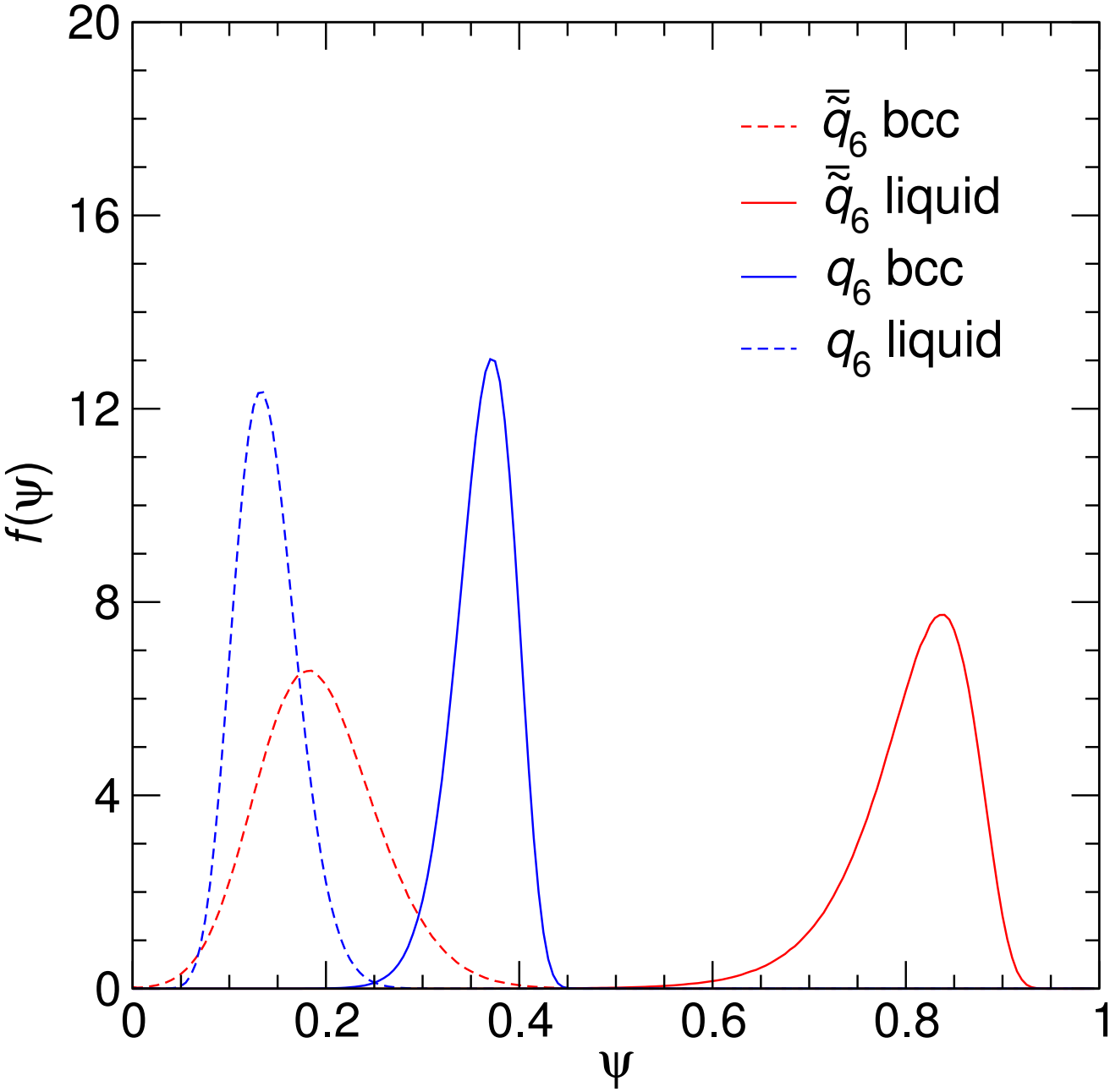
20
16
12
8
4
0
0
0.2
0.4
0.6
0.8
1
f(ψ)
ψ
$\tilde{\tilde{q}}_6$ bcc
$\tilde{\tilde{q}}_6$ liquid
q_6 bcc
q_6 liquid

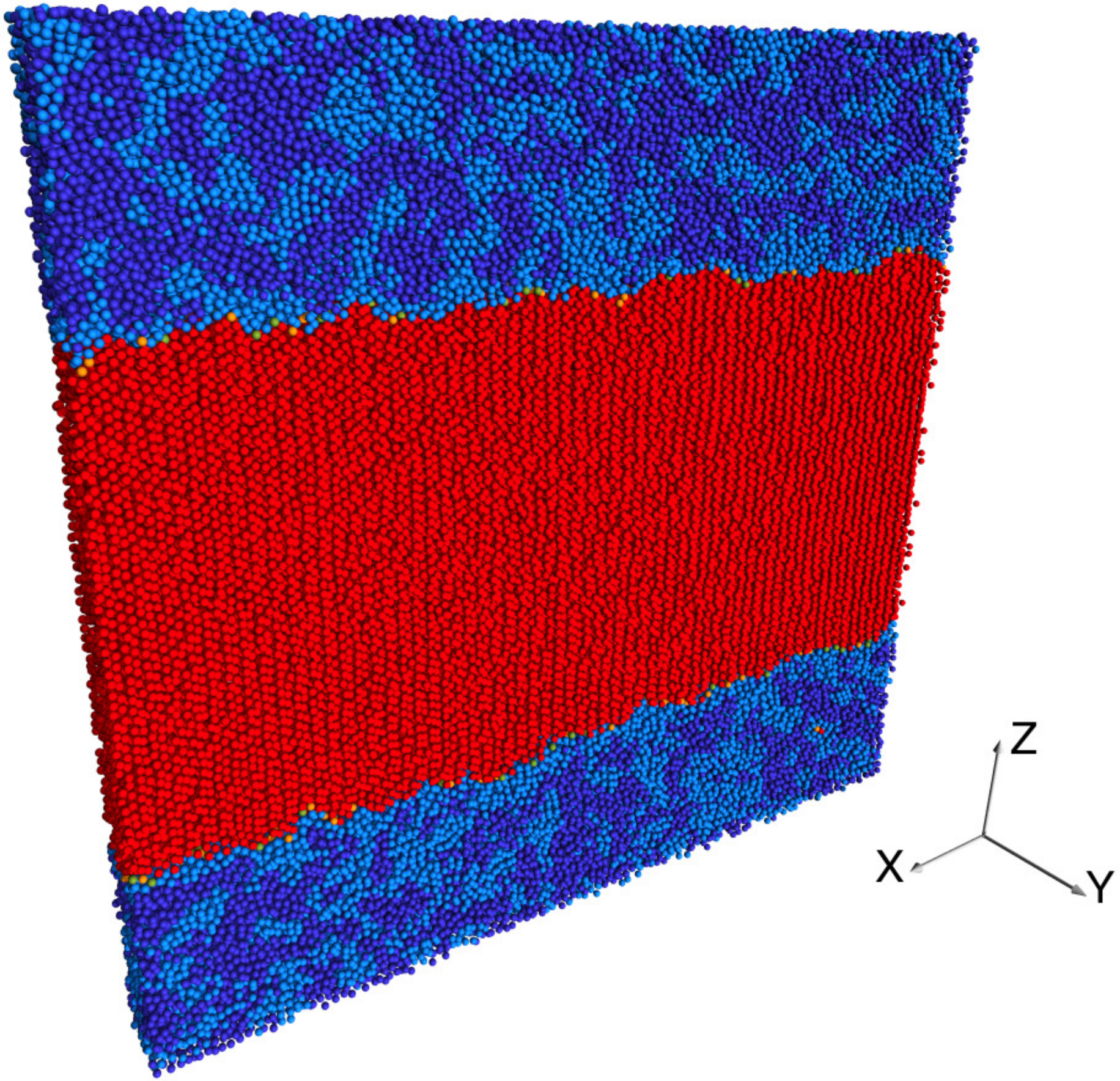
Z
X
Y

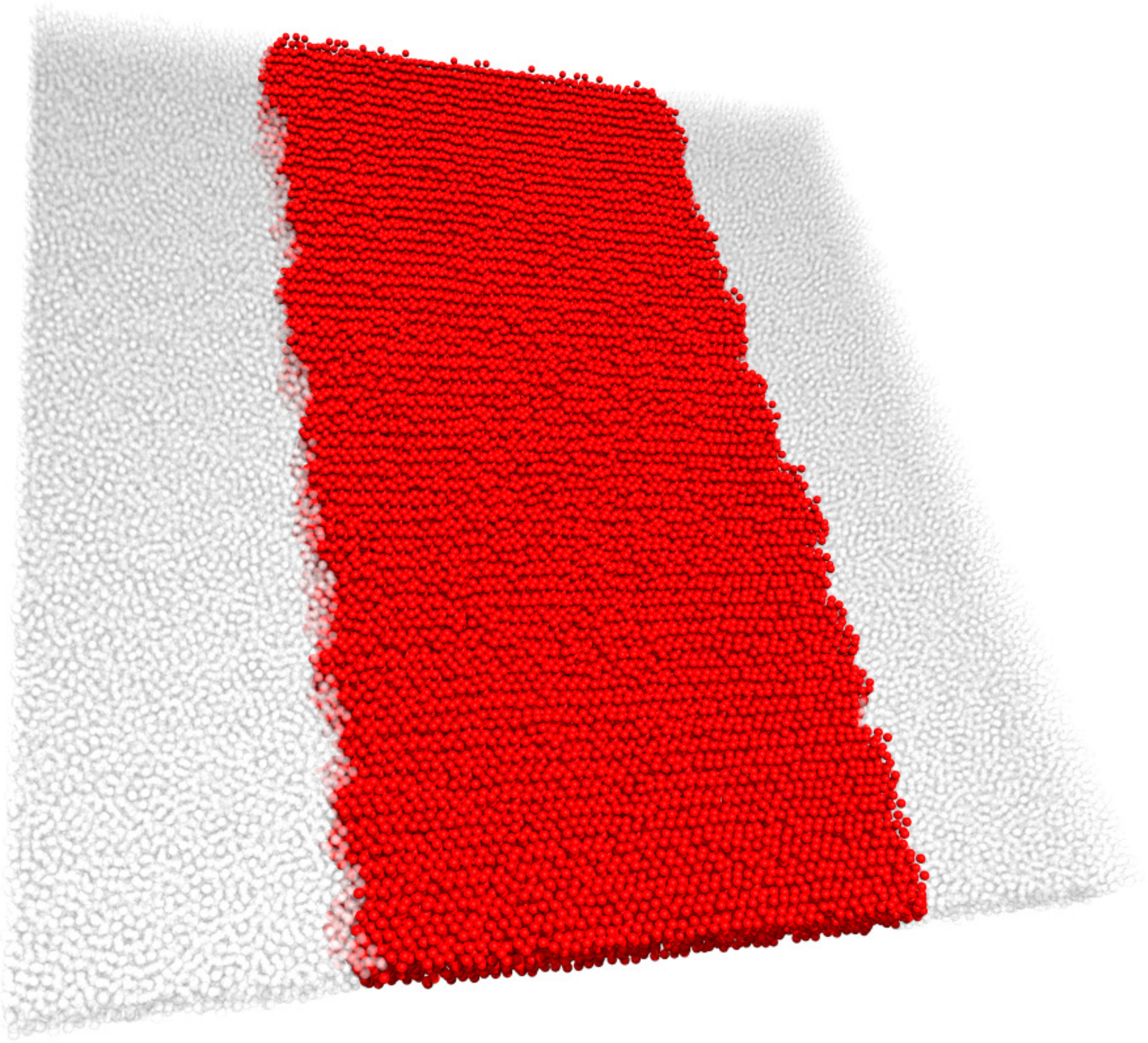

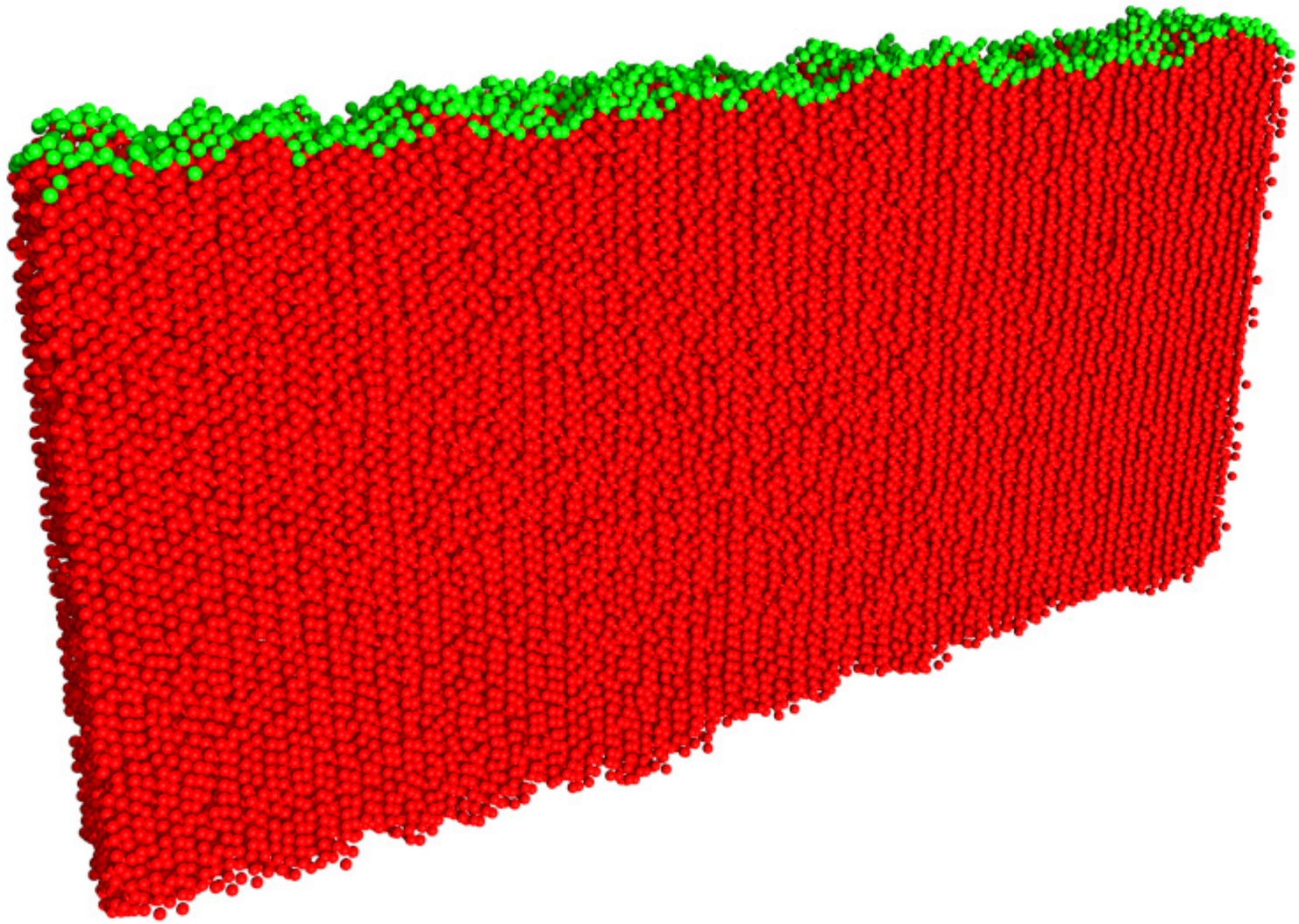

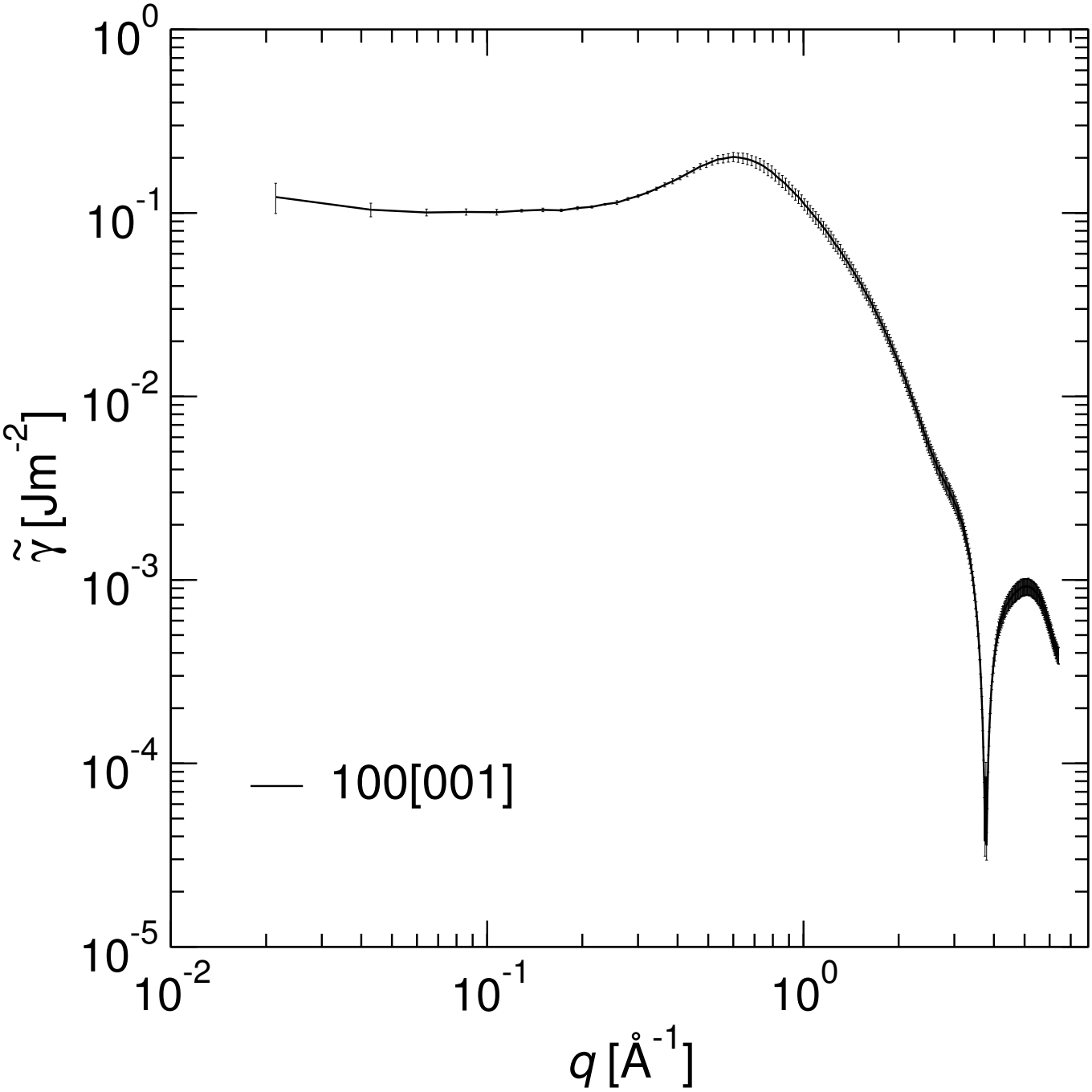
10^{0}
10^{-1}
10^{-2}
10^{-3}
10^{-4}
10^{-5}
$\tilde{\gamma}$ [Jm^{-2}]
100[001]
10^{-2}
10^{-1}
10^{0}
q [Å^{-1}]

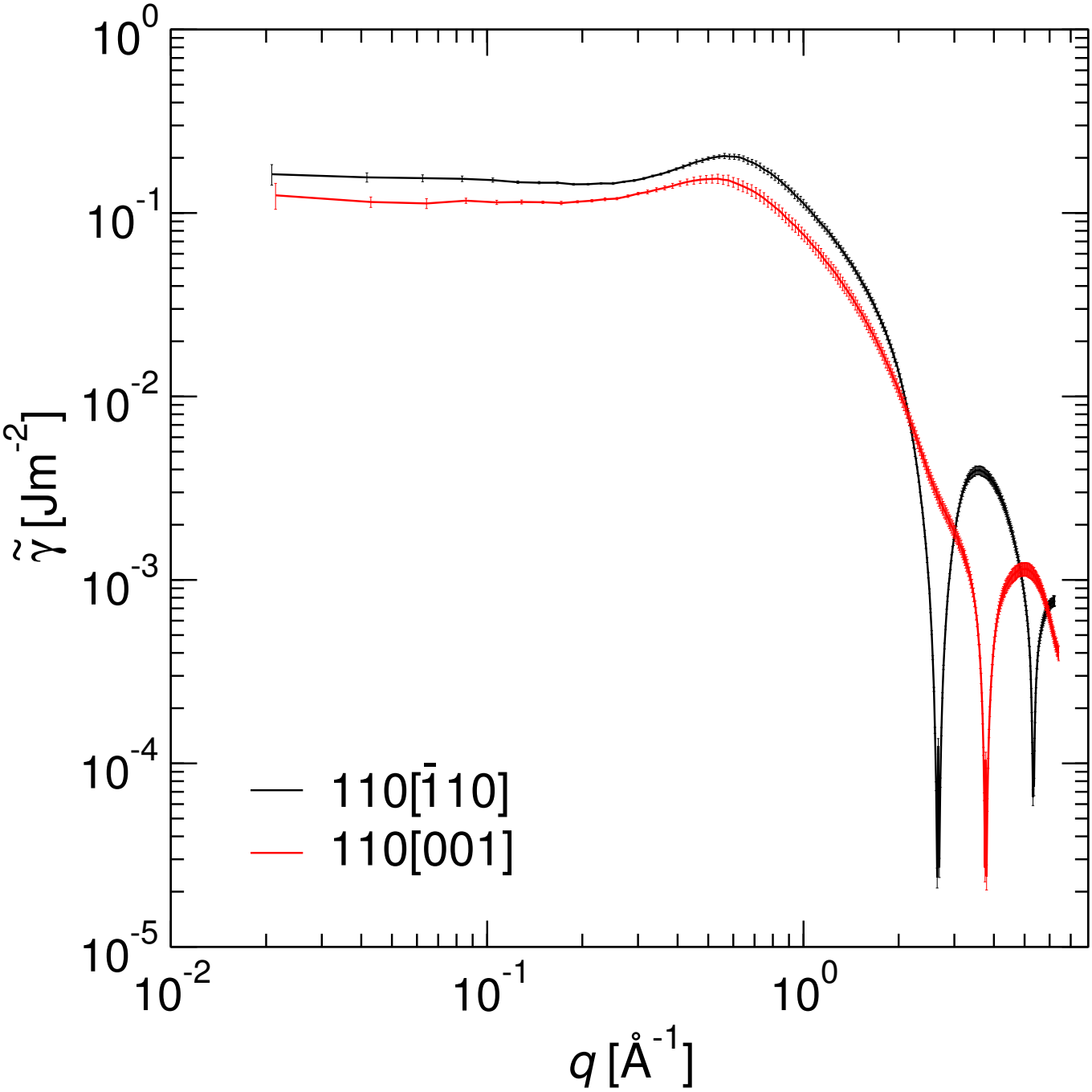
10^{0}
10^{-1}
10^{-2}
10^{-3}
10^{-4}
10^{-5}
$\tilde{\gamma}$ [Jm^{-2}]
10^{-2}
10^{-1}
10^{0}
q [Å^{-1}]
110[$\bar{1}$10]
110[001]

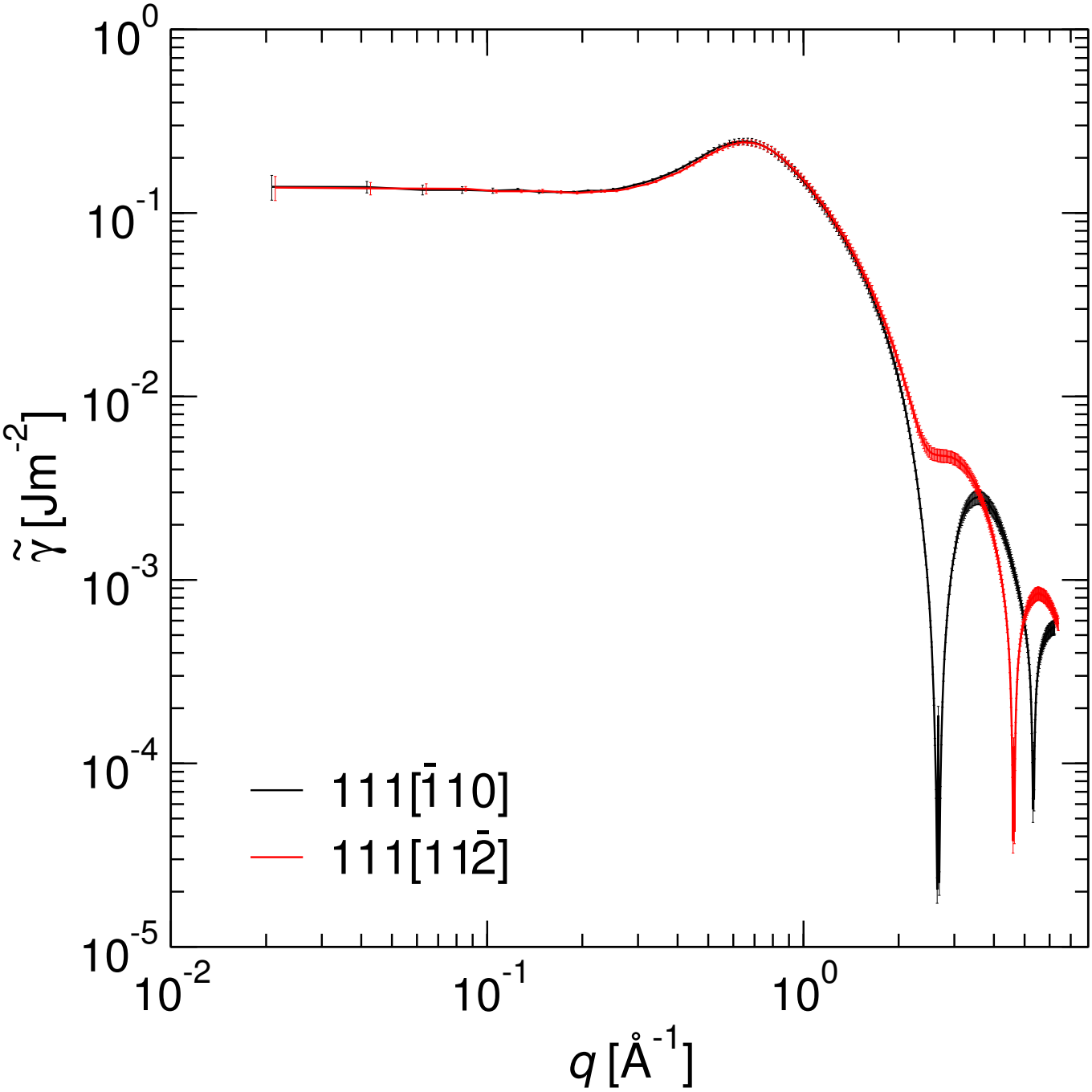
10^{0}
10^{-1}
10^{-2}
10^{-3}
10^{-4}
10^{-5}
$\tilde{\gamma}$ [Jm^{-2}]
10^{-2}
10^{-1}
10^{0}
q [Å^{-1}]
111[$\bar{1}$10]
111[11$\bar{2}$]

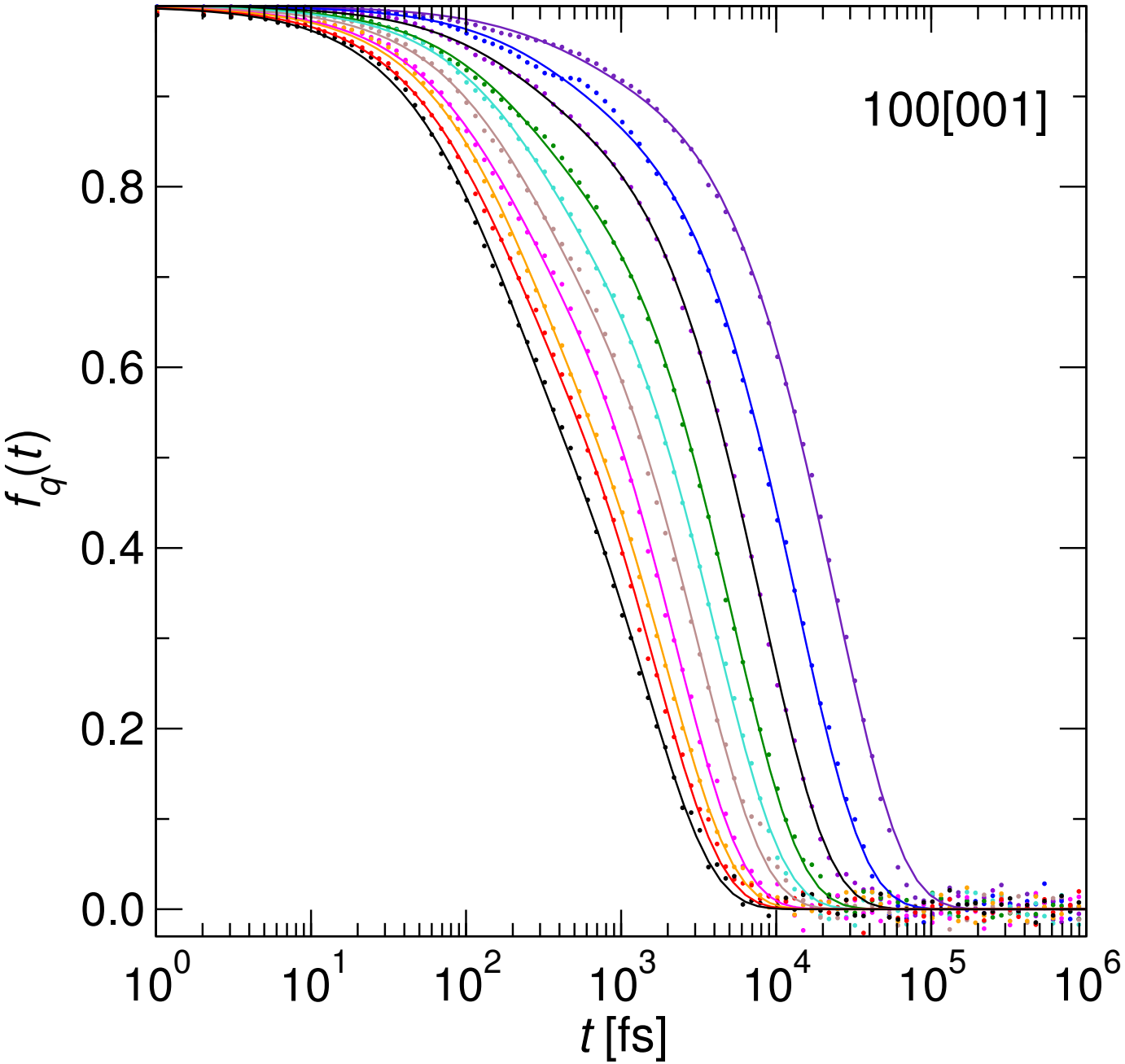
100[001]
$f_q(t)$
0.0
0.2
0.4
0.6
0.8
10^0
10^1
10^2
10^3
10^4
10^5
10^6
t [fs]

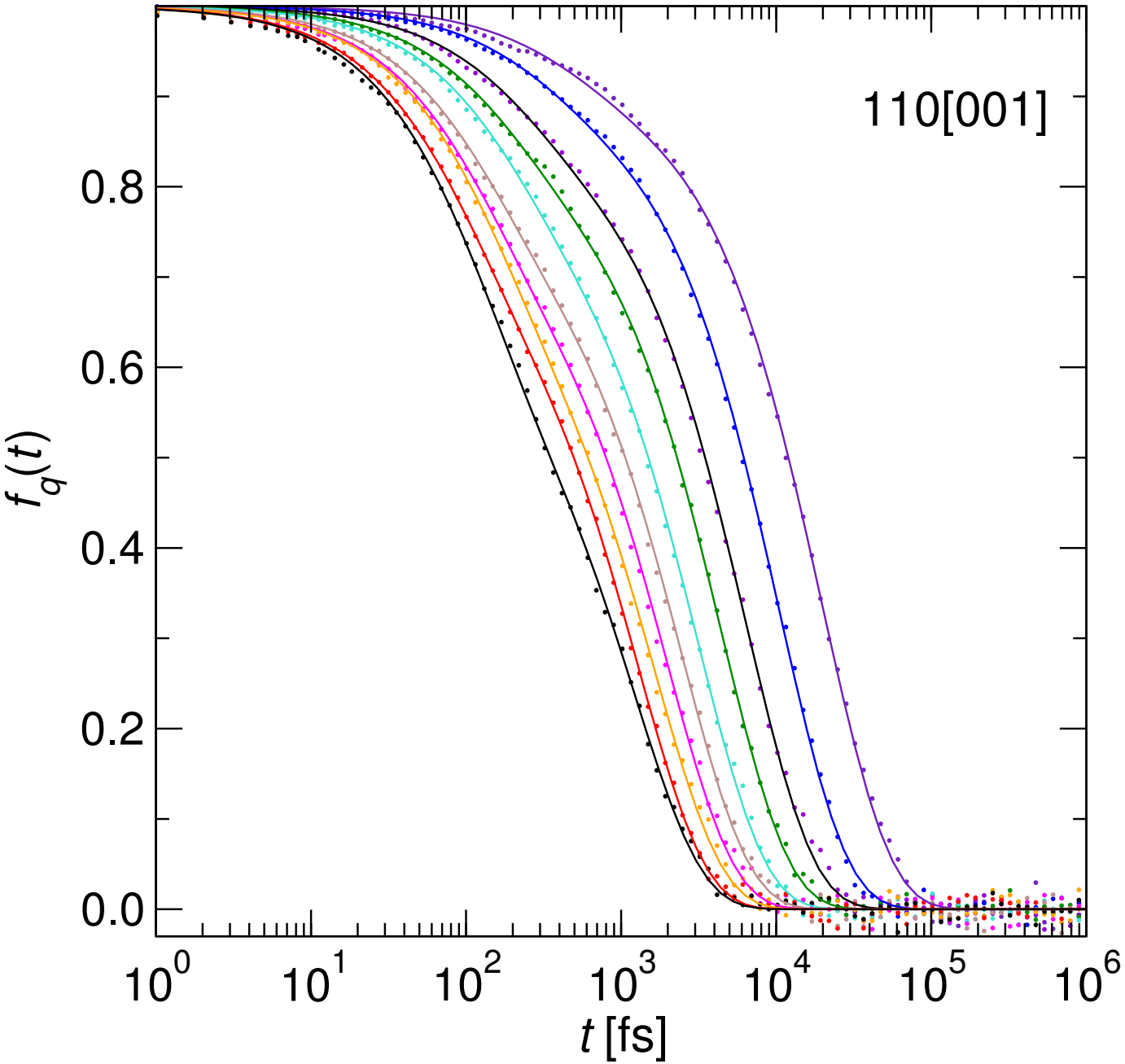
110[001]
0.8
0.6
0.4
0.2
0.0
$f_q(t)$
10^0
10^1
10^2
10^3
10^4
10^5
10^6
t [fs]

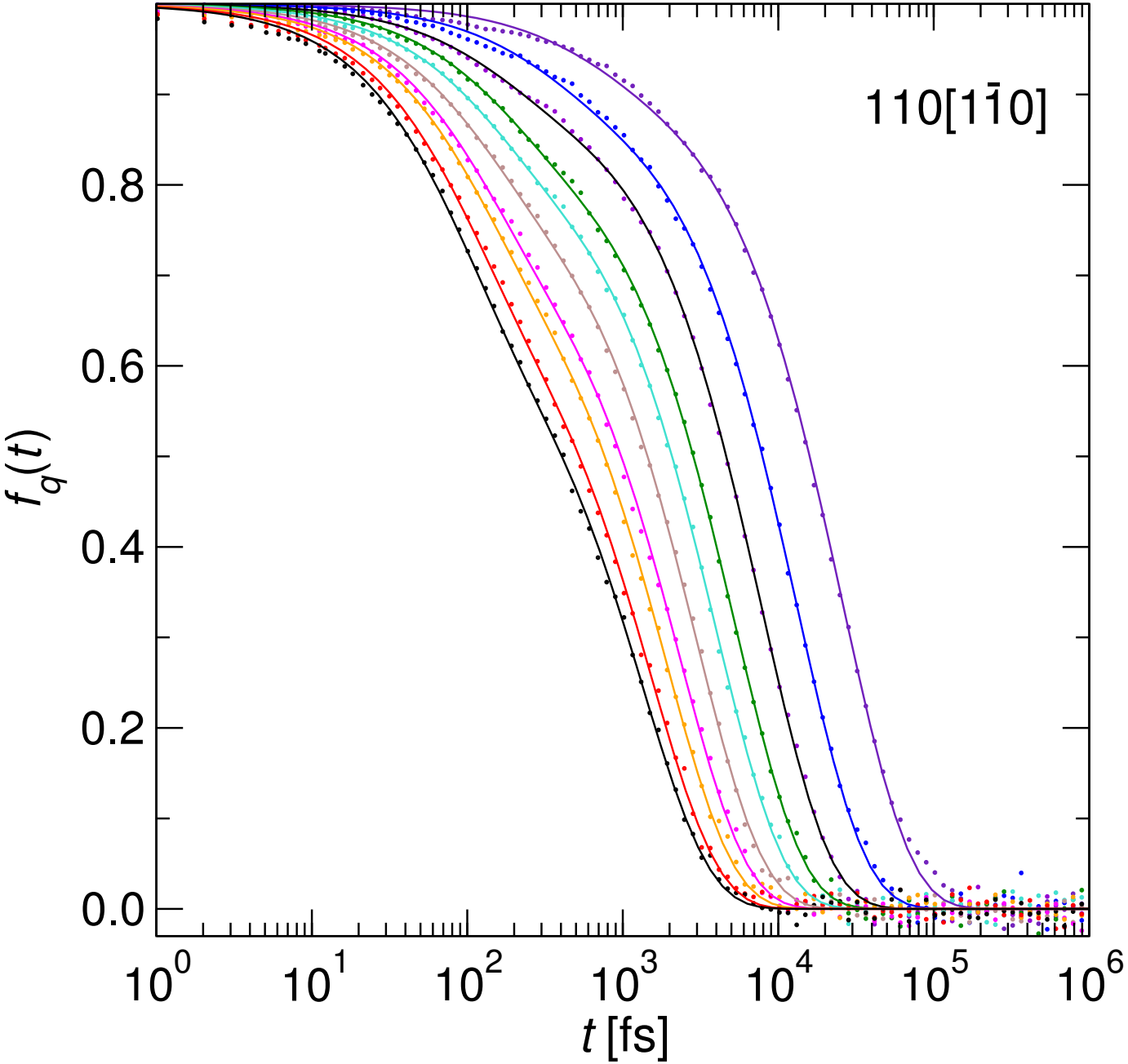
110[1$\bar{1}$0]
$f_q(t)$
0.0
0.2
0.4
0.6
0.8
10^0
10^1
10^2
10^3
10^4
10^5
10^6
t [fs]

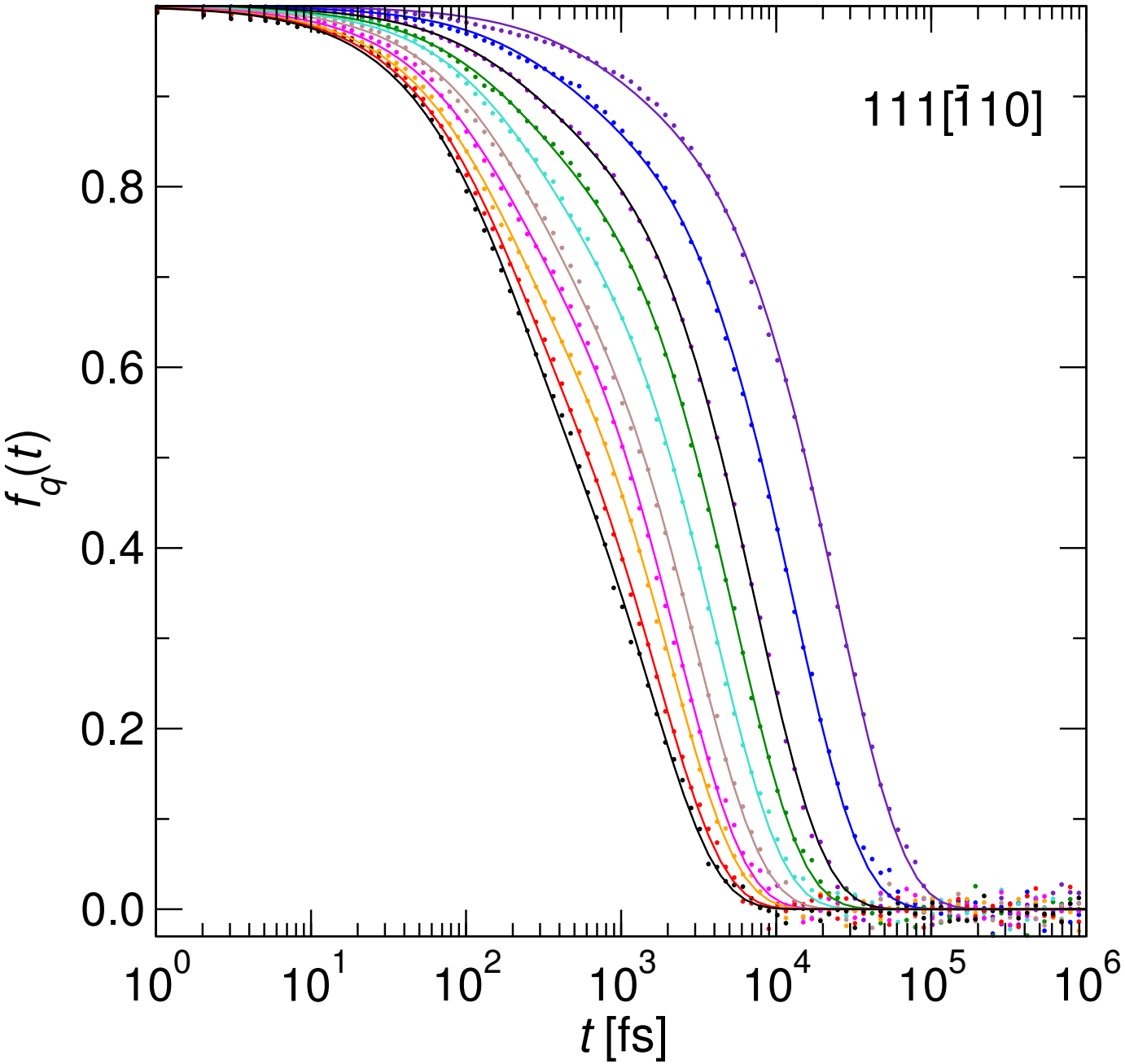
111[$\bar{1}$10]
0.8
0.6
0.4
0.2
0.0
$f_q(t)$
10^0
10^1
10^2
10^3
10^4
10^5
10^6
t [fs]

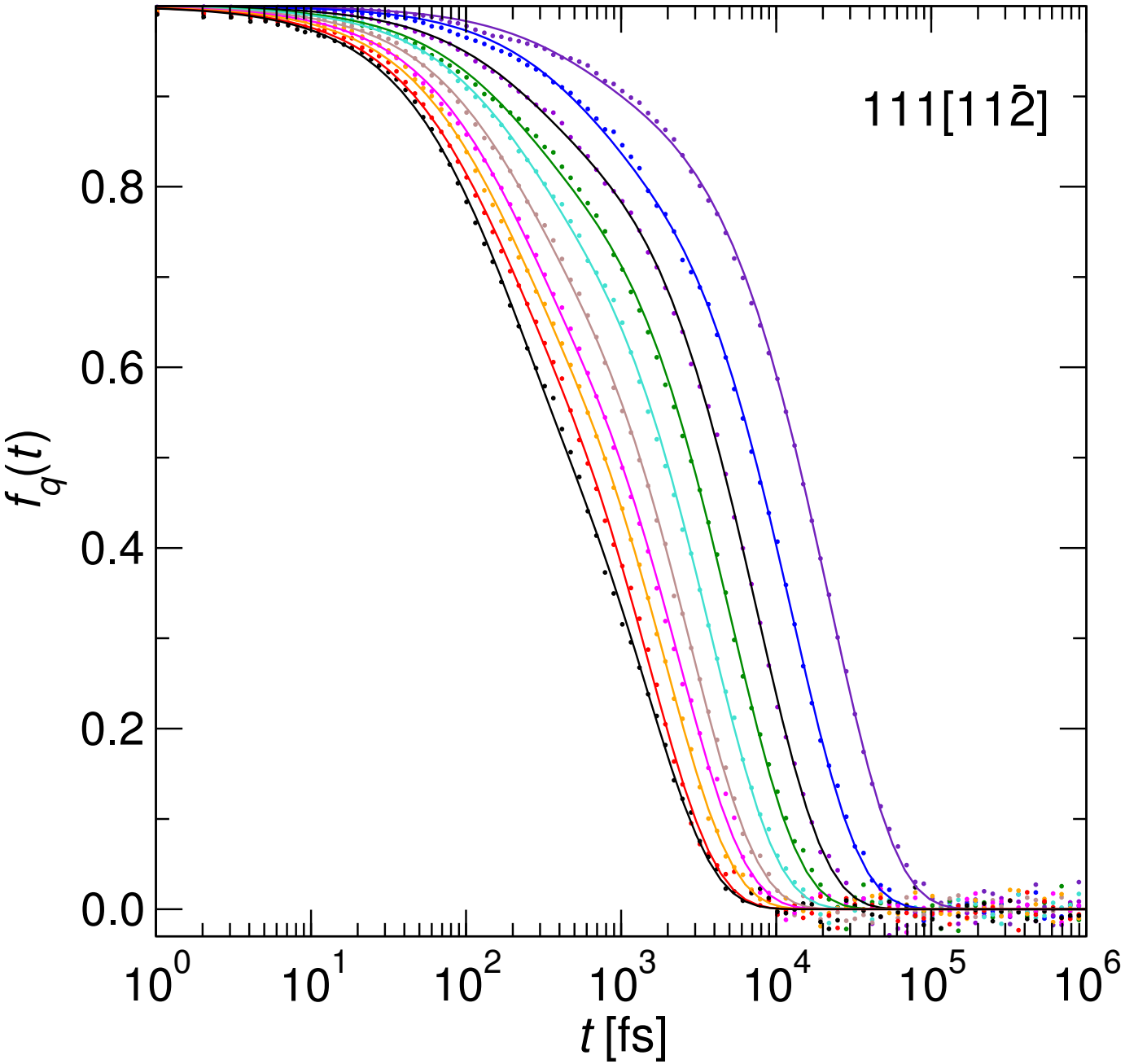
111[11$\bar{2}$]
$f_q(t)$
0.0
0.2
0.4
0.6
0.8
10^0
10^1
10^2
10^3
10^4
10^5
10^6
t [fs]

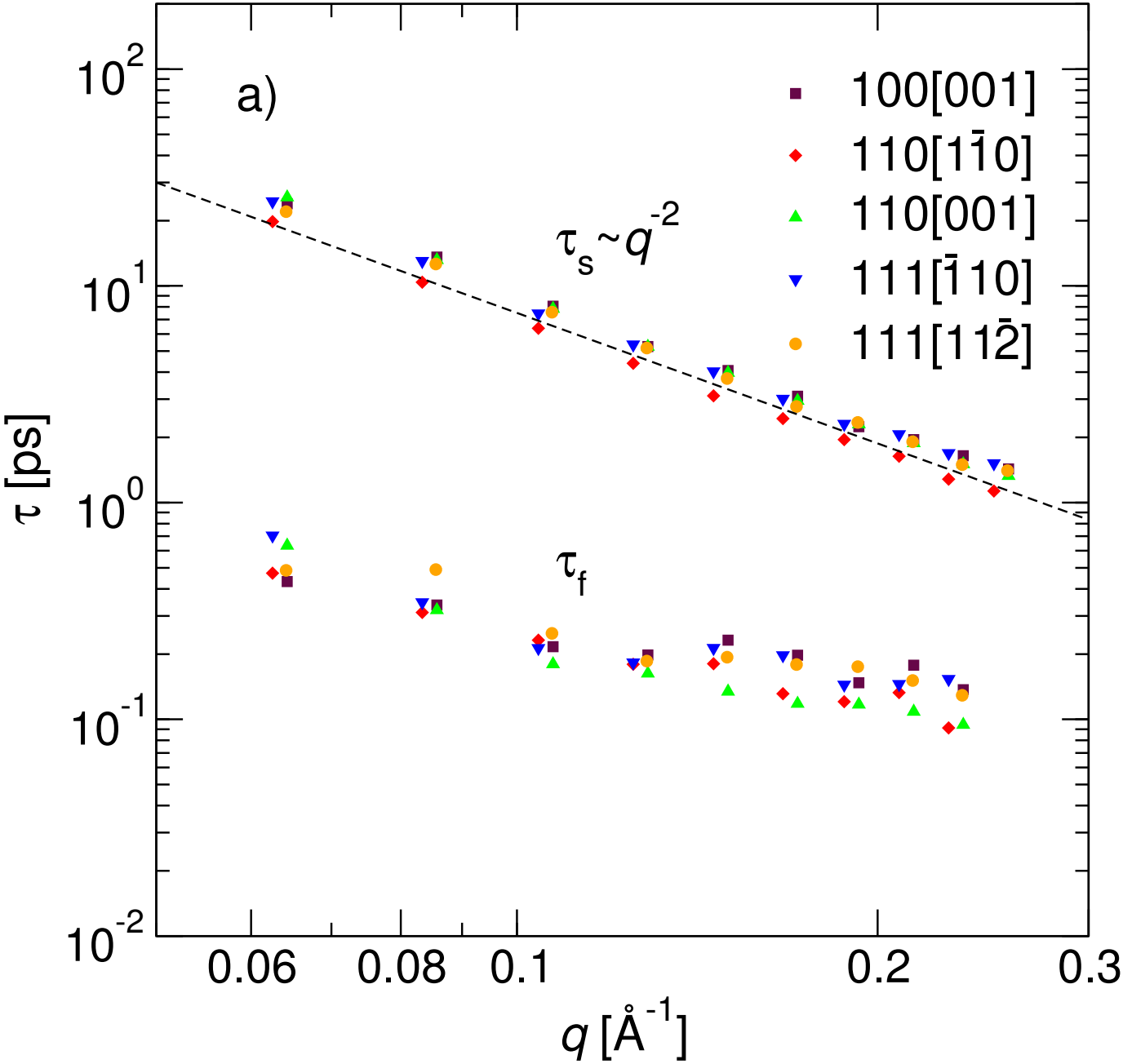
a)
100[001]
110[1$\bar{1}$0]
110[001]
111[$\bar{1}$10]
111[11$\bar{2}$]
$\tau_s \sim q^{-2}$
τ_f
τ [ps]
q [Å^{-1}]
10^2
10^1
10^0
10^{-1}
10^{-2}
0.06
0.08
0.1
0.2
0.3

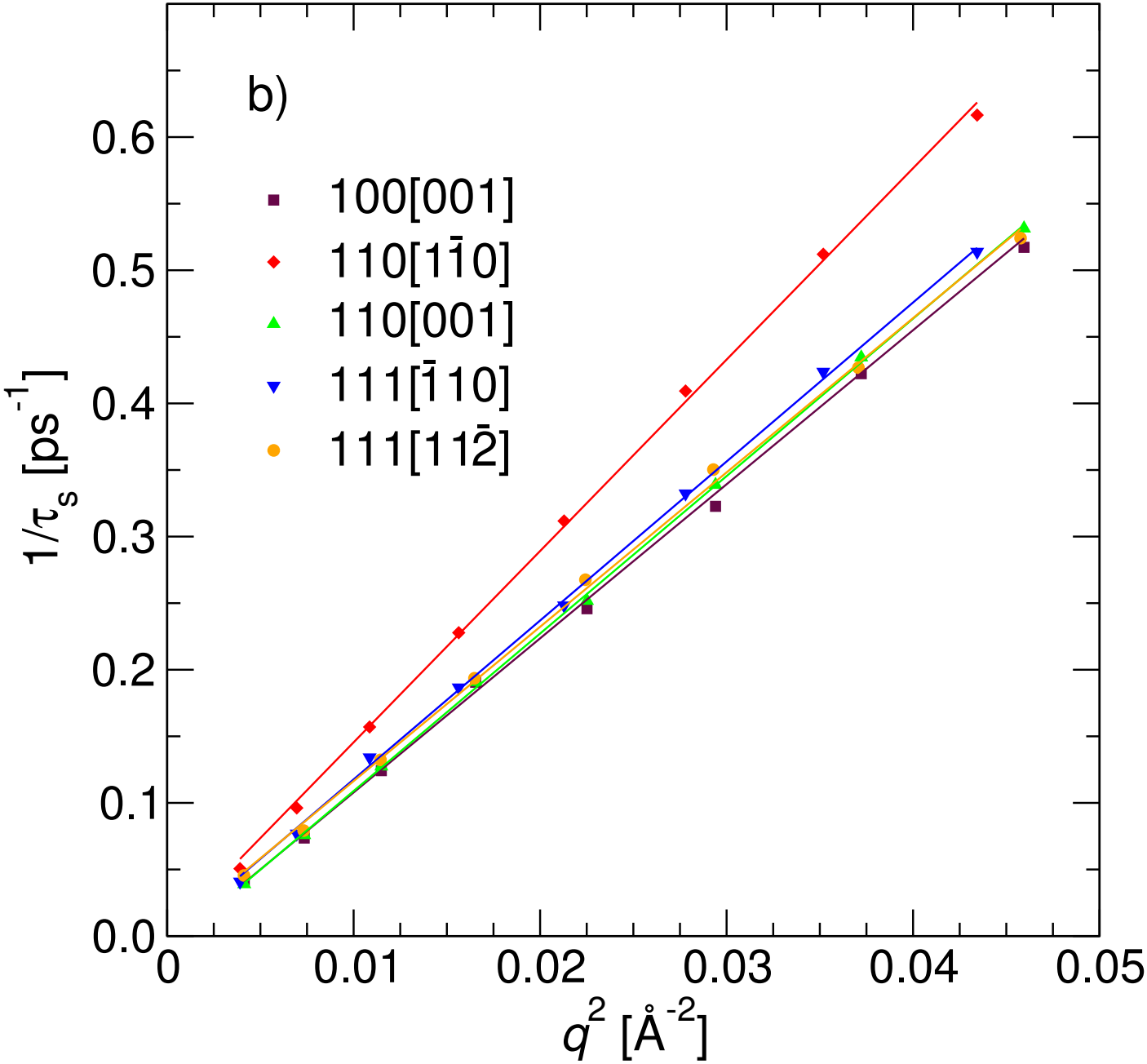
b)
100[001]
110[1$\bar{1}$0]
110[001]
111[$\bar{1}$10]
111[11$\bar{2}$]
0.0
0.1
0.2
0.3
0.4
0.5
0.6
0
0.01
0.02
0.03
0.04
0.05
$1/\tau_s$ [ps^{-1}]
q^2 [Å^{-2}]